RWTH Aachen

Department of Computer Science
Technical Report

Proceedings of the 1st GI Expert Talk on Localization

Mathias Pelka, Jó Ágila Bitsch, Horst Hellbrück and Klaus Wehrle
(Editors)

ISSN 0935–3232 · Aachener Informatik-Berichte · AIB-2015-08

RWTH Aachen · Department of Computer Science · Mai 2015 (revised version)

The publications of the Department of Computer Science of *RWTH Aachen University* are in general accessible through the World Wide Web.

`http://aib.informatik.rwth-aachen.de/`

Proceedings of the

1st GI Expert Talk on Localization

Lübeck, Germany
24 April 2015

CoSA Center of Excellence

ITG VDE

FACH HOCHSCHULE LÜBECK

COM SYS

RWTH AACHEN UNIVERSITY

Editors: Mathias Pelka, Jó Ágila Bitsch, Horst Hellbrück and Klaus Wehrle

Cover Picture: The cover was prepared by Jó Ágila Bitsch as a derivative work of *View over Lübeck April 2009* by Arne List, available under a Creative Commons Attribution-ShareAlike License 3.0 Unported available at `http://commons.wikimedia.org/wiki/File:View_over_L%C3%BCbeck_April_2009.jpg`.

Publisher: Department of Computer Science of *RWTH Aachen University*

ISSN 0935-3232

This is issue **AIB-2015-8** of the series **Aachener Informatik-Berichte**, appearing 24 April 2015, available online from
`http://aib.informatik.rwth-aachen.de/`

Printed in Germany

Message from the Chairs

Localization has become a major key technology in the field of medical, industrial and logistics applications. Especially indoor applications can benefit, e.g. the knowledge, where personnel are required, scarce resources are scattered, and goods are moving. Similarly, autonomous vehicles require reliable localization information for a wide range of task. Localization information in such places can save lives, time and money. However, there is no overall easy solution that covers all use cases. With the 1st GI Expert Talk on Localization we aim to provide a forum for the presentation and discussion of new research and ideas in a local setting, bringing together experts and practitioners. As a result, a considerable amount of time is devoted to informal discussion.

In addition to traditional localization topics such as radio based localization, we also aimed at novel technologies by encouraging submissions offering research contributions related to algorithms, stability and reliability, and applications. As a result the program includes a diverse set of contributions, ranging from phase and range based radio technology approaches, topological simplifications and clustering schemes, as well as automotive applications, including visual localization approaches.

A great deal of effort has gone into putting together a high-quality program. We thank all authors who submitted papers to this Expert Talk, and who ultimately made this program possible.

We express our appreciation to Fachhochschule Lübeck for its support, CoSA for the organization of the meeting, RWTH Aachen University for their additional help as well as GI and KuVS for bringing us together.

April 2015 Mathias Pelka, Jó Ágila Bitsch, Horst Hellbrück & Klaus Wehrle

Event Chairs

Horst Hellbrück, Lübeck University of Applied Sciences
Klaus Wehrle, RWTH Aachen University

Coordinators

Mathias Pelka, Lübeck University of Applied Sciences
Jó Ágila Bitsch, RWTH Aachen University

Table of Contents

Contributions

Useful Information

InPhase: An Indoor Localization System based on Phase Difference Measurements

Yannic Schröder, Georg von Zengen, Stephan Rottmann, Felix Büsching and Lars Wolf
Institute of Operating Systems and Computer Networks
Technische Universität Braunschweig
Email: [schroeder|vonzengen|rottmann|buesching|wolf]@ibr.cs.tu-bs.de

***Abstract*—Localization is an important challenge for all applications with autonomous navigating devices. Systems like GPS solve this challenge for most outdoor applications but such systems are not able to operate indoors. Indoor localization therefore is an active research topic. When it comes to locating nodes that travel from indoors to outdoors most systems are overwhelmed. Thus, we propose a system capable to localize nodes in such applications by using COTS transceiver chips. We utilize the phase measurement unit to perform distance measurements.**

I. Introduction

For highly automated cars it is crucial to know their own position to be able to navigate. In normal outdoor conditions the challenges of localization are solved by systems like Global Positioning System (GPS). Thinking of indoor and mixed environments like parking garages, most of the challenges are not satisfactorily solved by now. Of course, the use cases for such localization techniques are not limited to automotive applications. For example, logistics applications and industrial-used mobile robots also need such information.

In all these applications the localization is supposed to be as low cost as possible by retaining the accuracy. Therefore, most devices have resource constraints, which make localization of nodes a challenging task. Due to these constrains complex measurements like Time Difference of Arrival (TDoA) are not possible as only a single transceiver is available. As described by Boukerche et al. [1] different transmission channels like a radio pulse and a ultrasonic pulse are needed to realize this kind of TDoA measurements. TDoA measurements can also be realized using multiple transceivers for the same channel at different locations which results in rather large devices. Some transceivers support Time of Arrival (ToA) measurements but using this for ranging is complicated as a highly synchronized clock between the nodes is needed.

We propose an indoor localization system that fulfills the special requirements for resource constrained devices. It is capable to work with COTS transceiver chips like the AT86RF233 [2] by Atmel. Due to its measurement range, it can be used in both, indoor and outdoor scenarios. Therefore, it is capable to cover mixed application scenarios where nodes travel from indoors to outdoors and vice versa.

The remainder of this paper is structured as follows. In the next section we describe existing approaches to identify the advantages and disadvantages. Afterwards we give an overview of our proposed system and its inner workings to measure the distance between two nodes. Section IV investigates the challenges of estimating a position from the measured distances. Finally, we present the setup for a competition we participate in and also some lessons learned.

II. Related Work

Several methods for distance measurements have been proposed. Many applications typically use one of these approaches: Received Signal Strength Indicator (RSSI)-based, time-based or phase-based measurements. In this section, we will briefly introduce them.

A. RSSI

Basically, the strength of a radio signal decreases with the distance between transmitter and receiver. The remaining received power might be an indicator for the distance. In real world scenarios, this simple approach does not work well due to reflections which result in constructive or destructive interference. Even in outdoor scenarios with a direct line of sight between transmitter and receiver, these reflections occur, e.g. on the ground.

Although it is hard to calculate the distance to a single transmitter only based on the RSSI, so called fingerprinting can be applied which leads to reasonable results. If the RSSI of beacons from multiple fixed stations like WLAN access points can be received at the same time, these values can be stored in a central database. Later the node which needs to know its position, submits RSSI values of its neighbors to the database which answers with the position. Changes in the environment (disappearing stations, ...) lead to inaccurate positions, even moving object like cars will have an influence.

B. Time

Every radio signal transmitted travels with the (medium-specific) speed of light through space which means that the propagation time can also be used as an indicator for the distance. For this, two variants have to be distinguished, Time of Arrival (ToA) and Time Difference of Arrival (TDoA) [3]. If both, the transmitter and the receiver have highly synchronized clocks, the signal's time of flight can be calculated if the receiver knows the exact time when the signal was sent. The latter method, TDoA, measures either the ToA between multiple receiving nodes or at one single node the ToA of signals with different propagation speeds, like ultrasound and radio waves [4]. The Global Positioning System (GPS) run by the United States government is another example using the TDoA method. In this case, the receiving node uses the different transit times of signals from satellites with a known

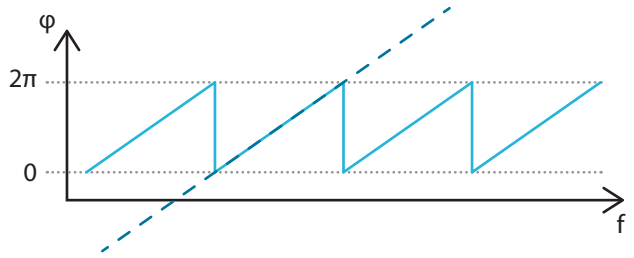

Fig. 1. Ideal phase response from PMU used for distance calculation. The indicated slope is proportional to the distance between the nodes.

position. For civil use, the accuracy of the position is about 15 m. To improve the performance of the system, Differential Global Positioning System (DGPS) can be used. In this case, an additional base station with a known position transmits the error of the position usually via a local short range radio links.

C. Phase

In the near field, the magnetic and electrical field components of electromagnetic transmitters are not in phase [5]. If a receiver is able to measure both components of a signal individually, the wavelength can be used to calculate the distance between sender and receiver. Large wavelengths are needed for precise measurements which result in huge antennas which may be a problem for small sensor nodes.

Another option is to measure the phase difference of signals with two signals between a transmitter and receiver. If it is possible to transmit or receive at two frequencies at the same time, no synchronization of clocks is required [6].

It is also possible to measure the phase difference of signals sent sequentially [7]. No absolute synchronization between transmitter and receiver is needed. Depending on the frequency offset, either high ranges or a high accuracy can be achieved with these measurements.

The approach shown in this paper uses the same method, but we use more measurement steps and apply calculations on the data which leads to a good result of the phase measurements for distance estimation.

III. Distance Measurement

Our system consists of multiple INGA [8] sensor nodes forming a Wireless Sensor Network (WSN). The sensor nodes are equipped with an AT86RF233 [2]. This is an IEEE 802.15.4 compliant transceiver chip that features a PMU.

We have implemented the Active Reflector (AR) method as proposed by Kluge and Eggert [9] as distance sensor for the Contiki operating system [10]. The AR method uses two wireless sensor nodes to measure the phases of a transmitted continuous wave signal between them.

For an AR measurement two nodes are needed. In our setup we use an *anchor* and a *tag*. In the first step the *anchor* acts as receiver and measures the phase of the signal transmitted by the *tag*. To mitigate the effect of unsynchronized clocks both nodes switch roles after the first measurement. Therefore, in the second step the *tag* measures the phase of the signal transmitted by the *anchor*. As both transceiver's Phase Locked

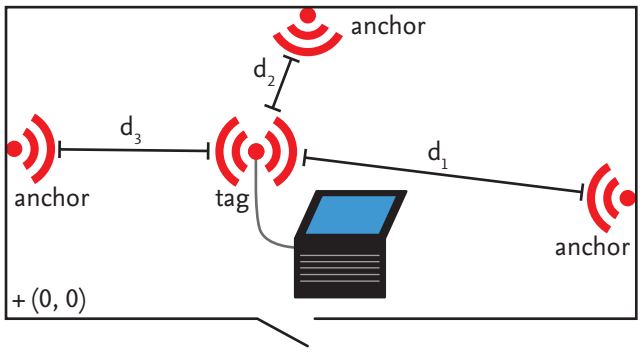

Fig. 2. Example deployment of our system in a sample room. Three fixed nodes are used as *anchors*. A fourth *tag* is connected to a portable computer.

Loops (PLLs) run at the same frequency in transmission and reception mode, any phase difference due to not synchronized clocks is irrelevant.

A schematic plot of such a measurement is shown in Figure 1. The dashed blue line represents the slope of the phase response (solid blue line) of the channel measured by the system. This slope is proportional to the distance between the nodes. To start a measurement, we designed a protocol where the *tag* asks an *anchor* to participate in a measurement of the channel's phase response. After the measurement is completed, the results stored at the *anchor* are transmitted to the *tag*. This phase measurement is repeated with different *anchors* deployed at known positions.

By estimating the similarity of the measured phase response with an ideal saw tooth signal our system calculates a Distance Quality Factor (DQF). This DQF is used to decide whether the measurement should be used for position calculation or if it is not good enough.

IV. Position Estimation

After performing distance measurements to multiple *anchors*, the position of the *tag* is computed. We employ a heuristic solver based on Sequential Least Squares Programming [11] for this task. This solver tries to minimize an error function for the *tag's* position. The bounding box of the area where the system is deployed and a starting position for the optimization is used as input for the solver. This starting position is either the last position of the *tag* if the optimization was successful or a generic starting point otherwise. The error function takes the measured distances d_n, the known positions of the *anchors* and the designated *tag's* position from the solver as input. From this input the distances between *tag* and *anchors* are calculated. Then, the relative errors to the measured distances d_n are calculated. The error function does not use all measured distances and *anchors* but only the ones with the best quality as indicated by the DQF. The sum of these errors is returned to the solver for further optimization. The solver evaluates the error function multiple times to find a local minimum of the error function. When the optimization is completed and successful, the calculated position of the *tag* is returned. This position can then be displayed to a user or used for other purposes.

V. COMPETITION

With our system we participate in the *Microsoft Indoor Localization Competition* at the *IPSN 2015*. Figure 2 shows the minimal deployment our system needs to be able to work. The competition area has of course a more complex shape and also includes multiple rooms. Depending on the size and layout of the area to cover at least three *anchors* are needed. As permitted by the competition's rules, we will deploy ten *anchors* over the whole area. Our *anchors* are mounted to the walls of the setup area. The position of the *anchors* must be measured as exactly as possible to ensure an accurate localization of the *tag*.

The *anchors* are placed carefully to ensure maximum coverage of the area. For valid measurements a direct line of sight between the *anchors* and the *tag* is required. The availability of the line of sight is critical as measurements through objects other than air will result in distance errors. Due to the directional antenna design of the INGA sensor node it is crucial that the predominant directions of the antennas are pointing at each other. To mitigate this requirement the tag features an omnidirectional antenna. This allows arbitrary placement of the tag without the requirement to align it to the anchors. However, the anchor's antennas must still point at the tag to ensure a valid measurement. All sensor nodes are placed at the same height to further reduce the effect of the directional antennas.

The *tag* is connected to a portable computer. The measurement data is sent to this device where the position is calculated and the result is displayed.

REFERENCES

[1] A. Boukerche, H. Oliveira, E. Nakamura, and A. Loureiro, "Localization systems for wireless sensor networks," *Wireless Communications, IEEE*, vol. 14, no. 6, pp. 6–12, December 2007.

[2] *Low Power, 2.4GHz Transceiver for ZigBee, RF4CE, IEEE 802.15.4, 6LoWPAN, and ISM Applications*, 8351st ed., Atmel Corporation, San Jose, August 2013.

[3] A. Boukerche, H. A. Oliveira, E. F. Nakamura, and A. A. Loureiro, "Localization systems for wireless sensor networks," *Wireless Commun.*, vol. 14, no. 6, pp. 6–12, Dec. 2007. [Online]. Available: http://dx.doi.org/10.1109/MWC.2007.4407221

[4] A. Savvides, C.-C. Han, and M. B. Strivastava, "Dynamic fine-grained localization in ad-hoc networks of sensors," in *Proceedings of the 7th Annual International Conference on Mobile Computing and Networking*, ser. MobiCom '01. New York, NY, USA: ACM, 2001, pp. 166–179. [Online]. Available: http://doi.acm.org/10.1145/381677.381693

[5] H. Schantz, "Near field phase behavior," in *Antennas and Propagation Society International Symposium, 2005 IEEE*, vol. 3B, July 2005, pp. 134–137 vol. 3B.

[6] T. Nowak, M. Hierold, A. Koelpin, M. Hartmann, H.-M. Troger, and J. Thielecke, "System and signal design for an energy-efficient multi-frequency localization system," in *Wireless Sensors and Sensor Networks (WiSNet), 2014 IEEE Topical Conference on*, Jan. 2014, pp. 55–57.

[7] M. Pelka, C. Bollmeyer, and H. Hellbrück, "Accurate radio distance estimation by phase measurements with multiple frequencies," in *2014 International Conference on Indoor Positioning and Indoor Navigation*, Oct. 2014.

[8] F. Büsching, U. Kulau, and L. Wolf, "Architecture and evaluation of INGA - an inexpensive node for general applications," in *Sensors, 2012 IEEE*. Taipei, Taiwan: IEEE, October 2012, pp. 842–845. [Online]. Available: http://www.ibr.cs.tu-bs.de/papers/buesching-sensors2012.pdf

[9] W. Kluge and D. Eggert, "Ranging with IEEE 802.15.4 narrow-band PHY," https://mentor.ieee.org/802.15/dcn/09/15-09-0613-01-004f-ranging-with-ieee-802-15-4-narrow-band-phy.ppt, September 2009.

[10] A. Dunkels, B. Gronvall, and T. Voigt, "Contiki - a lightweight and flexible operating system for tiny networked sensors," in *Local Computer Networks, 2004. 29th Annual IEEE International Conference on*, November 2004, pp. 455–462.

[11] D. Kraft *et al.*, *A software package for sequential quadratic programming*. DFVLR Obersfaffeuhofen, Germany, 1988.

Range-based Weighted-likelihood Particle Filter for RSS-based Indoor Tracking

Zan Li, Andreea Hossmann-Picu, Torsten Braun
Institute of Computer Science and Applied Mathematics, University of Bern, Switzerland
Email:li@iam.unibe.ch, hossmann@iam.unibe.ch, braun@iam.unibe.ch

***Abstract*—Attractive business cases in various application fields contribute to the sustained long-term interest in indoor localization and tracking by the research community. Location tracking is generally treated as a dynamic state estimation problem, consisting of two steps: (i) location estimation through measurement, and (ii) location prediction. For the estimation step, one of the most efficient and low-cost solutions is Received Signal Strength (RSS)-based ranging. However, various challenges – unrealistic propagation model, non-line of sight (NLOS), and multipath propagation – are yet to be addressed. Particle filters are a popular choice for dealing with the inherent non-linearities in both location measurements and motion dynamics. While such filters have been successfully applied to accurate, time-based ranging measurements, dealing with the more error-prone RSS-based ranging is still challenging. In this work, we address the above issues with a novel, weighted likelihood, bootstrap particle filter for tracking via RSS-based ranging. Our filter weights the individual likelihoods from different anchor nodes exponentially, according to the ranging estimation. We also employ an improved propagation model for more accurate RSS-based ranging, which we suggested in recent work. We implemented and tested our algorithm in a passive localization system with IEEE 802.15.4 signals, showing that our proposed solution largely outperforms a traditional bootstrap particle filter.**

I. Introduction

In the last years, research on the topic of indoor localization and tracking has become increasingly important, motivated by the shortcomings of the Global Positioning System (GPS) indoors but also by the attractiveness of business cases in various application fields such as Ambient Assisted Living (AAL), home automation, and security. Wireless technologies have emerged as candidates for indoor localization due to their ubiquitousness. Particularly, WiFi is currently the dominant local wireless network standard for short-range communication in indoor environments and is the leading technology for indoor localization. An alternative technology is ZigBee, a wireless standard for short-range communication with low power consumption. ZigBee is used in most urban area wireless sensor networks, which are vital components of today's smart city programs. It is also widely used in home automation and industry applications. Therefore, it has attracted interests of researchers as an alternative to WiFi localization.

Based on the target's participation, indoor positioning systems can be classified as *active localization* systems and *passive localization* systems. In active localization, target devices participate actively in the localization process. In contrast, in a passive localization system, the targets (which are also sources of packets) do not need to participate in the localization process. Instead, several Anchor Nodes (ANs) are deployed to passively overhear the packets from tracked devices. A server can be used to collect useful information, e.g., RSS, from different ANs and to run localization algorithms. Since ZigBee devices typically have limited resources (energy and computational power), we focus here on passive localization systems, as they have the advantage of not using any of the target's resources. In addition, they are also very attractive for third-party providers of positioning and monitoring services.

Range-based localization and tracking using RSS information is an efficient and low cost solution for a passive localization system. However, due to unrealistic propagation models (e.g. typically the Log Distance Path Loss (LDPL) model), non-line of sight (NLOS) and multipath propagation, high accuracy ranging is still challenging. As a consequence of the inaccuracy of RSS-based ranging, the resulting indoor localization and tracking may also be low accuracy. Once acquired, the ranging information is converted into the coordinates of the target, possibly via a method that is robust to ranging errors. In static scenarios, trilateration algorithms are employed.

For mobile targets, Bayesian filters are one of the most popular and high accuracy solutions. Bayesian filters (e.g. Kalman filter, particle filter) estimate the position of the mobile target by constructing prediction and measurement equations. A Kalman filter assumes that all error terms and measurements are Gaussian-distributed and the system is linear. An Extended Kalman Filter (EKF) can deal with nonlinear models via Taylor series expansion. However, it is only a suboptimal solution and requires a Gaussian model of the measurement and state transition noises. To handle both the non-linearity and the non-Gaussian properties, particle filters are employed [1]. Several works have investigated particle filters for tracking, primarily in areas where accurate location measurements are possible, such as time-based localization, pedestrian dead reckoning with inertial sensors [2], fingerprinting, and data fusion [3]. However, there is little work investigating range-based particle filters relying solely on the more error-prone RSS in complex indoor environments. The authors of [4] investigated range-based particle filters using RSS in an outdoor environment. They provided a particle filter with summation of the likelihoods for the range measurements from different ANs. Their results show $4m$ to $6m$ accuracy, which is often not accurate enough for indoor tracking.

In this work, the main contribution is a novel range-based weighted-likelihood particle filter, solely relying on RSS for indoor tracking. By weighting the likelihoods for different ANs based on their ranging outputs, our proposed particle filter impressively mitigates the influence of ranging errors and improves the tracking accuracy. Additionally, to improve ranging accuracy, we adopt a Non-Linear Regression (NLR)

model to relate the measured RSS information to ranges instead of the traditional LDPL model.

II. Range-based Particle Filter Preliminaries

In this section, we introduce the preliminaries for particle filters and state the problems for the range-based particle filter solely relying on RSS.

To define the problem of tracking, the target state vector x_k should be estimated from the measurements $z_{1:k}$, which are collected from different ANs up to discrete time k. The state vector, x_k consists of the coordinates and moving speed of the target. For range-based tracking, the measurements z_k comprise the range information from different ANs. Based on the Bayesian estimation framework, the relationships between the state vector x_k and the measurement z_k are as follows:

$$x_k = f(x_{k-1}, v_k), \tag{1}$$

$$z_k = h(x_k, u_k), \tag{2}$$

where v_k is the noise for state transition and u_k is the measurement noise. Equation (1) is the prediction function and Equation (2) is the measurement function.

One of the most widely used particle filters is Bootstrap Particle Filter (BPF). Based on Monte Carlo methods, the posterior Probability Density Function (PDF) $p(x_k|z_{1:k})$ can be estimated by the following delta function:

$$p(x_k|z_{1:k}) \approx \sum_{i=1}^{N_s} w_k^i \delta(x_k - x_k^i), \tag{3}$$

where x_k^i is the ith particle and w_k^i is the associated weight. N_s is the total number of particles. For BPF, the weight of each particle can be calculated as:

$$w_k^i \propto w_{k-1}^i \cdot p(z_k|x_k^i), \tag{4}$$

where $p(z_k|x_k^i)$ is the measurement likelihood of z_k for x_k^i.

Therefore, an efficient and accurate derivation of the likelihood function $p(z_k|x_k^i)$ is essential for accurate tracking by BPF. z_k is comprised of range information from N different ANs, i.e., $z_k = [d_1, d_2, \cdots, d_N]$. Assuming that the range information from different ANs are independent from each other, a typical likelihood can be written as

$$p(z_k|x_k^i) = \Pi_{j=1}^{N} p(d_j|x_k^i). \tag{5}$$

In this case, the likelihoods for the estimated ranges from different ANs are treated equally and this kind of particle filter is referred to as the traditional BPF in the remainder of the paper. Different from time-based localization with specific signals, which benefits from high accuracy ranging, RSS-based localization normally suffers from large ranging errors. Hence, z_k normally deviates from the real values, which makes the likelihood $p(z_k|x_k^i)$ deviate from the real likelihood. Correspondingly, the weight associated to each particle is inaccurate, which results in inaccurate location estimation.

III. Range-based Tracking Algorithms Design

As introduced in Section II, RSS-based ranging BPF for indoor tracking is challenging because of the inaccurate ranging information. Therefore, in this section, we will introduce our methods for improving ranging accuracy and mitigating the influence of inaccurate ranging on the likelihood. After introducing a more realistic propagation model, to reduce as much as possible the ranging error, we describe our proposal for correcting the likelihoods of the particle filter.

A. Non-linear Regression Model

The LDPL model has been demonstrated to be an inaccurate model in indoor environments. In our previous work [5], we propose to model the relationship between the RSS values and propagation distances as a nonlinear curve fitting problem. Hence, we provide a nonlinear regression (NLR) model as,

$$d = \alpha \cdot e^{\beta \cdot RSS} \tag{6}$$

where d is the propagation distance, RSS is the received power, α and β are two unknown parameters in the model that need to be obtained from some initial measurements.

Given N_t training positions in the initial measurements, (d_n, RSS_n) are collected at the nth training position. We apply the nonlinear least square criterion, in which the sum of squared residuals should be minimized as,

$$\underset{(\alpha,\beta)}{\operatorname{argmin}} \sum_{n=1}^{N_t} (\alpha \cdot e^{\beta \cdot RSS_n} - d_n)^2. \tag{7}$$

To find the solution of this unconstrained optimization problem, the trust region algorithm [6] is applied, because it is robust and has a strong global convergence property.

Normally, all ANs in different locations adopt the same propagation model. However, the signal propagation from the target to different ANs are typically very different, and, thus, this oversimplification will introduce large estimation errors for indoor localization. Therefore, in our work, we calibrate the α and β pairs for different ANs.

B. Weighted Likelihood Particle Filter

After obtaining ranging information, a novel bootstrap particle filter, which adopts weighted multiplication of likelihoods for different ANs to mitigate the ranging error influence, is designed in our work to convert the range information to the coordinates of the target. For the BPF filter, the range outputs from the NLR model construct the measurement vector as $z_k = [d_1, d_2, \cdots, d_N]$. The coordinates (x, y) and moving speed $(\hat{x}, \hat{y})$ of the target construct the state vector $x_k = [x, y, \hat{x}, \hat{y}]$.

Assuming the range measurements from different ANs are independent, the likelihood $p(z_k|x_k^i)$ can be written as a multiplication of individual likelihoods from different ANs as Equation (5). In this form, all the likelihoods from different ANs are simply treated equally. As mentioned in Section II, ranging outputs are always biased and correspondingly the likelihoods from different ANs normally deviate from the real likelihoods. Furthermore, ranging errors from different ANs are normally different. Therefore, we propose to reduce the contribution of the likelihoods with large ranging errors

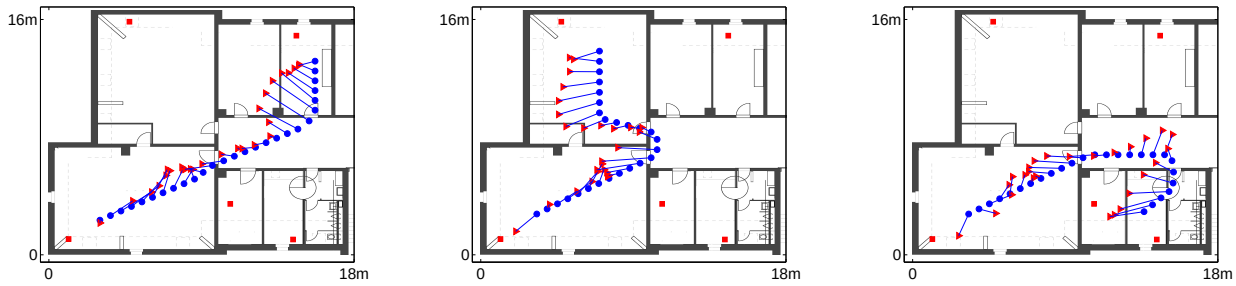

(a) The First Path (b) The Second Path (c) The Third Path

Fig. 1: Tracking in Different Paths
(Rectangular Points: ANs; Triangular Points: Estimated Positions; Circle Points: Ground Truth Positions)

to the whole likelihood $p(z_k|x_k^i)$. Therefore, we provide a Weighted-likelihood BPF (WBPF) with exponential weights on individual likelihoods from different ANs as:

$$p(z_t|x_k^i) = \Pi_{j=1}^{N} p(d_j|x_k^i)^{m_j}, \tag{8}$$

where m_j is the exponential weight for the likelihood of the jth AN. To reduce the contribution of the likelihoods with large ranging estimation that normally result in large ranging errors, the weight m_j should be inversely proportional to the range estimation as:

$$m_j = \frac{1/d_j}{\sum_{n=1}^{N} 1/d_n}. \tag{9}$$

IV. Measurement Setup and Evaluation

The proposed WBPF has been implemented in our passive localization testbed [7] for IEEE 802.15.4 signals. We conducted a set of measurements to evaluate our method.

A. Measurement Setup

The measurements were conducted on the third floor of the IAM building at University of Bern. Five ANs were deployed to capture IEEE 802.15.4 signals from a TelosB node. The target TelosB node periodically broadcasts 5 packets per second and the transmission power is configured to the maximum level (Level 31). The target TelosB node is held by a person in hand and moves along three different paths as shown in Figure 1. In the figure, the blue circle points indicate the ground truth positions of the moving paths and the red triangular points are the estimated positions. The moving speed is around $1m/s$ but the moving directions change for all the three moving paths. We aggregate the packets every 0.7 seconds to estimate one location along the moving path.

B. Measurement Results and Analysis

Figure 2 summarizes the Cumulative Distribution Function (CDF) of localization errors for our proposed WBPF and the traditional BPF. According to the results, our proposed WBPF significantly outperforms the traditional BPF. In more detail, after introducing the exponential weights to different individual likelihoods, our proposed WBPF can mitigate the influence of ranging errors and correspondingly improve the localization accuracy compared to the traditional BPF. WBPF improves the median error by 28.6% compared to BPF (from $2.1m$ to $1.5m$). 90% of the localization errors with WBPF are lower than $2.4m$, which outperforms BPF ($3.5m$) by 31.4%.

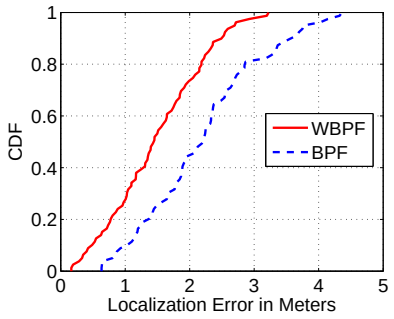

Fig. 2: CDF of Localization Errors with WBPF and BPF

V. Conclusions

In this paper, we proposed a novel particle filter (WBPF) using RSS-based tracking by exponentially weighting the individual likelihoods according to the estimated ranges. With the proposed algorithms, our tracking system for ZigBee signals achieves high accuracy with a median error of $1.5m$ and our proposed WBPF significantly outperforms the typical BPF.

References

[1] M. Arulampalam, S. Maskell, N. Gordon, and T. Clapp, "A tutorial on particle filters for online nonlinear/non-gaussian bayesian tracking," *Signal Processing, IEEE Transactions on*, vol. 50, no. 2, pp. 174–188, Feb 2002.

[2] F. Hong, Y. Zhang, Z. Zhang, M. Wei, Y. Feng, and Z. Guo, "Wap: Indoor localization and tracking using wifi-assisted particle filter," in *Local Computer Networks (LCN), 2014 IEEE 39th Conference on*, Sept 2014, pp. 210–217.

[3] J. Prieto, S. Mazuelas, A. Bahillo, P. Fernandez, R. Lorenzo, and E. Abril, "Adaptive data fusion for wireless localization in harsh environments," *Signal Processing, IEEE Transactions on*, vol. 60, no. 4, pp. 1585–1596, April 2012.

[4] Z. Shah, R. Malaney, X. Wei, and K. Tai, "Experimental deployment of particle filters in wifi networks," in *Communications, 2007. ICC '07. IEEE International Conference on*, June 2007, pp. 4692–4697.

[5] Z. Li and T. Braun, "A passive source localization system for ieee 802.15.4 signal," in *In The International Conference on Network Systems (NetSys) 2015 (Demostration Session)*, 2015.

[6] R. B. S. Richard H. Byrd and G. A. Shultz, "A trust region algorithm for nonlinearly constrained optimization," in *SIAM Journal on Numerical Analysis*, vol. 24, 1987, pp. 1152–1170.

[7] Z. Li, T. Braun, and D. Dimitrova, "A time-based passive source localization system for narrow-band signal," in *The IEEE International Conference on Communications (ICC)*, June 2015.

Towards Real-Time Network-Based Positioning in LTE

Islam Alyafawi*, Navid Nikaein†, and Torsten Braun*
*Communication and Distributed System Group, Universität Bern
{alyafawi, braun}@iam.unibe.ch
†Mobile Communications Department, EURECOM
navid.nikaein@eurecom.fr

***Abstract*—With the availability of smart handsets and increase in wireless bandwidth brought by cellular technologies such as LTE, the demand for location based services grows. The location information can be utilized for commercial services, network operations, or public safety requirements. LTE facilitates location services of user equipment (UE) by making use of UE network information as well as radio signals measured at the network. The serving network may support different localization methods transparent to the UE implementation and capabilities. In this paper, we discuss practical issues and challenges for deploying and evaluating network-based positioning and tracking in a real LTE network. More specifically, our focus is on small and indoor cells. We also bring insights on experimental results for indoor LTE setup.**

I. Introduction

When satellite technologies like GPS fail to provide a reasonable level of positioning accuracy in indoor and urban canyon environments, there is a need for a positioning method that can provide comparable results for rural and urban, city centers, outdoor and indoor environments. With the increasing number of LTE-capable mobile devices, users, network operators, service providers, and regulatory bodies are demanding for low-latency and accurate location-based services (LBS). As such, LTE requires an integrated positioning solution that effectively combines different positioning techniques and can meet a wide range of accuracy and performance requirements. Network-based positioning is an interesting approach for LBS since it is transparent to the UE [1]. It ensures a consistent and reliable positioning performance towards a wide range of UE manufacturers. However, position estimation can be achieved by taking measurements from at least three different cells. A main challenge in network-based positioning is signal overhearing. Unlike in GSM or CDMA, LTE radio is scheduled (by the serving cell) with different frequency and time allocations [2]. This unique architecture possesses a significant challenge on LTE for supporting network-based positioning.

The authors in [3] proposed to use a modified scheduling algorithm, which is of semi-persistent type, to set a known pattern of physical resource allocation for a UE of interest. In 3GPP Release 11, uplink transmission configuration can be shared between LTE base stations (eNBs) over the so-called, X2 interface. Hence, neighboring cells will be able to overhear the target UE transmission. As illustrated in Figure 1, the X2-interface does not require a dedicated physical connection between eNBs. It is a logical interface between neighboring cells carried over an existing IP transport network. X2 does not require significant bandwidth, however, it requires very short latencies across the backhaul of the network to achieve real-time coordination between eNBs. In this paper, we provide insights into the design of LTE cloud radio access network (C-RAN), as a possible approach to collect mobile network measurements and advanced technique for positioning and tracking mobile devices in real-time. Our focus on localization is small and indoor cells as both have an important part to play for location services especially in areas where mobile devices cannot directly determine their position through GPS alone.

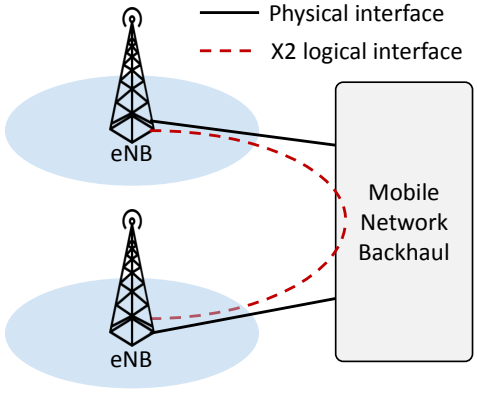

Fig. 1. The X2-interface.

II. Uplink Resource Allocation

In LTE eNB, a number of PHY and MAC layer parameters are jointly controlling the transmission's resource allocation for the eNB downlink and UE uplink through a scheduler [4]. There is no dedicated channel allocated between a UE and the serving eNB. Time and frequency resources are dynamically shared between UEs in downlink and uplink channels. Each 1 ms, the scheduler controls which UEs are supposed to receive data on the downlink/uplink shared channels and on which resource blocks (RBs). One RB occupies a bandwidth of 180 KHz and spans one slot of 0.5 ms. However, the schedule needs measurement reports about the downlink and uplink channel conditions to make a proper allocation and ensure high throughput. Our focus is on the uplink scheduler due to its importance for network-based positioning. In the uplink, the scheduler uses the following inputs to allocate radio resources for uplink transmission [2]: (i) UE buffer status report (BSR) indicates the amount of data available for transmission in the uplink buffers of the UE, (ii) UE power headroom report

(PHR) indicates the additional return power available at the UE, and (iii) channel quality indicator (CQI). CQI is obtained from uplink physical reference signals periodically sent by UEs, namely, sound reference signals (SRS), and from physical uplink shared channel (PUSCH). With this information, the eNB gets an idea about how much bandwidth a UE is able to use in a subframe. Before sending and receiving data, UEs need to know some information such as (i) the radio resource allocation, (ii) modulation and coding scheme and its corresponding transport block size, (iii) the timing advance alignment, and (iv) transmitting power level [2]. All this information is sent using downlink control information (DCI) from the serving eNB to the target UEs every 1 ms. Each DCI is identified by the target UE radio network temporary ID (RNTI) issued by the network.

A. X2-Interface

The X2 interface connects neighboring eNBs in a point-to-point fashion. X2 is a logical interface between neighboring eNBs and can be switched over the existing backhaul network. The X2 interface consists of two parts: (i) Control-Plane (C-Plane) responsible for establishment and release of tunnels neighboring eNBs to allow data tunneling, and (ii) User Plane (U-Plane), which supports the tunneling of end user packets between the eNBs and minimize packet losses due [5].

In cellular networks, UEs might be heard by more than one eNB. The UE connects to the eNB with the strongest signal and interferes with cells that are operating on the same frequency, which become more severe with heterogeneous network deployments. The applicability of the X2-interface indeed has several practical implementation aspects as well as operational challenges on the network side, such as (i) compatibility for X2 support must exist in all eNB collaborating in the positioning process (cooperating set), (ii) due to high frequent configuration of the radio resources (every 1 ms), eNB cooperating set must be tightly synchronized and connected to each other through high throughput and low latency backhaul link connection. For lowest X2 latency, the physical X2 connection, driven by the transport technology (e.g. optical fiber, microwave or copper-based technologies), should be as short as possible.

III. The C-RAN Solution

In the LTE architecture called cloud RAN (C-RAN), the cellular area is covered by multiple remote radio heads (RRHs) responsible for transmitted and received radio signals. All baseband processing units (BBUs), as well as radio resources scheduling, is typically migrated to a farm of high-performance computing data centers and connected to their RRHs using a fronthaul adapter. C-RAN advantages compared to conventional RANs are scalability and flexibility of further RRH deployment [6]. Deployment of C-RAN BBUs in data centres is possible through different virtualization techniques, such as the Linux container (LXC). An excellent use case for C-RAN is to share network contextual information, e.g., channel conditions, the downlink control information (DCI), or UE statistics, between BBUs of nearby geographical RRHs. To be specific, our aim is to use the high bandwidth connection between the host running the virtual switch (or shared memory) and VMs running the C-RAN as a replacement of the X2-interface, or what we call now, the X2-like interface. The size of DCI field varies between 3-4 bytes. The synchronous nature of C-RAN BBUs brings some gains for the LTE X2-like interface such as reduced signalling overhead and close-to-instantaneous DCI information exchange between BBUs.

One use-case envisioned by the X2-like interface is network-based positioning. Our main target is to exchange DCI allocation between different BBU instances using a C-RAN solution in a virtual environment. In this paper, we consider the OpenAirInterface (OAI) software implementation of LTE. The OAI, developed by EURECOM, is an open-source software defined radio (SDR) implementation of LTE including both the RAN and the evolved packet core (EPC) [6].

IV. Network-Based Positioning

Many methods have been developed to achieve network-based positioning with different positioning accuracies such as cell-ID with round trip time (RTT), TA or uplink time difference of arrival (UTDoA) [1]. It is shown that positioning techniques on the base of the network particularly appear to overcome many weak points of UE-based techniques:

- Minimize the impact on UE manufacturer and supported protocols (UE agnostic).
- Take advantages of higher hardware reliability and accuracy for collecting radio measurements.
- Collect radio measurements in the correct direction; giving that downlink and uplink radio measurements are not always reciprocal [8].
- Allow accessing fine-grained radio measurements for various desired positioning accuracy.

In LTE, both the UE and the eNB are required to perform all necessary measurements to properly characterize radio channels and ensure the transmission's QoS. Measurements are used for a variety of purposes including cell selection, scheduling, handover, power control, and positioning services [8]. We present only eNB radio measurements, which are supported by all standard eNB implementations and are interested for us to perform network-based positioning: (i) power measurements, such as received signal strength indicator (RSSI), and RSSI per active subcarrier, (ii) time measurements, such as timing advance (TA), and (iii) quality measures, such as channel quality indicator. Each UE sends back its scanning report to the serving eNB with the reference signal received power/quality (RSRP/RSRQ) of the serving and neighbour cells [2].

In this work, we rely on power measurements based on our previous experience of challenges facing indoor time measurements. Moreover, the TA resolution is limited to 0.52 μs, which is equivalent to 78.12 m. This distance is longer than the separation distance between eNBs in our experimental setup. We use an advanced RSSI-based positioning techniques based on our previous work [7].

V. Experimental Setup and Evaluation

An indoor cloudified LTE network is built based on the OAI hardware and software platforms to evaluate the performance of network-based positioning for LTE. One UE

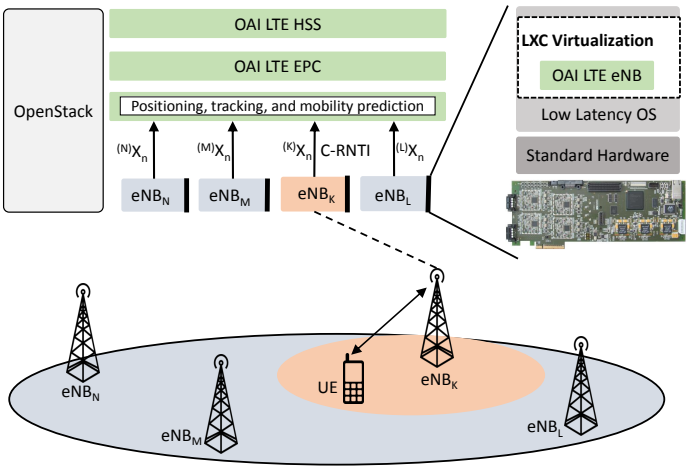

Fig. 2. Experimental setup.

and four OAI eNBs connected to one OAI EPC and one OAI home subscriber server (HSS) are used, as illustrated in Figure 2. To build a cloudified LTE network, we ported the OAI eNB, EPC, and HSS into LXC environment as the virtualization technology under the control of OpenStack. All the machines (hosts or guests) operate on Ubuntu 14.04 with the low-latency Linux kernel version 3.17 for x86-64 architectures. eNBs are configured to operate at 5 MHz in band 7 with frequency division duplex (FDD) mode and a single antenna. In the considered setup, each eNB is running on a separate PC interconnected with the EPC through the S1 interface. Furthermore, each eNB streams the real-time radio measurement X_n information to a localization algorithm located at the same PC running the EPC, where n is the number of measurements.

We acquire data into sets X_n of 30 sec duration. The UE was considered static during the acquisition time, whereas each experiment spans a duration of 5 min. The final positioning results are expressed in Figure 3. Blue squares represent the real UE position and black circles represent the estimated UE positions. Without any special hardware, any prior knowledge of the indoor layout and any offline calibration of the system, our system using RSSI measurements obtains an average positioning error of 2.7 meters with a deployment density of 0.89 base stations per 100 square meters. The same system using RSRP measurements reported by the target UE obtains an average error of 3.3 meters.

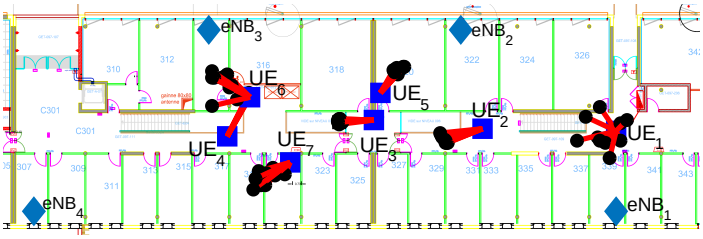

Fig. 3. Network-based performance.

VI. Conclusion

To obtain a cost-efficient, accurate and real-time positioning solution, we proposed the use of network-based positioning in LTE. We presented some challenges facing network-based positioning, mainly, the signal overhearing by neighbouring cells. We presented our solution using X2-like interface in C-RAN and run a set of experiments in a real indoor environment. Without any prior knowledge of the indoor layout and any offline calibration of the system, results show an average positioning error of 2.7 m using the proposed network-based approach with a deployment of 0.89 base stations per 100 square meters.

References

[1] White Paper. *SPIRENT, LTE Positioning Technology for Mobile Devices: Test Challenges and Solutions*, 2012.

[2] E. Dahlman, S. Parkvall, and J. Skld. *4G LTE/LTE-Advanced for Mobile Broadband*, Academic Press, UK, 2011.

[3] L. Telefonaktiebolaget and I. Siomina. *Ensuring positioning quality-of-service for lte positioning*, Google Patents, 2013.

[4] G. Berardinelli, L. R. de Temino, S. Frattasi, M. Rahman, and P. Mogensen. *OFDMA vs.SC-FDMA: Performance Comparison in Local Area IMT-a Scenarios*, IEEE Wireless Communications, 2008.

[5] White Paper. *Backhauling X2*, Cambridge Broadband Networks Limited, 2010.

[6] I. Alyafawi, et. al. *Critical Issues of Centralized and Cloudified LTE-FDD Radio Access Networks*, ICC, 2015.

[7] I. Alyafawi, D. C. Dimitrova, and T. Braun. *SDR-based Passive Indoor Localization System for GSM*, ACM SIGCOMM Software Radio Implementation Forum (SRIF), 2014.

[8] H. Holma and A. Toskala. *LTE for UMTS – OFDMA and SC–FDMA Based Radio Access*, John Wiley & Sons, Inc., 2009.

Adhoc Topology retrieval using USRP

Chuong Thach Nguyen
University of Goettingen, Germany
chuongthach.nguyen@stud.uni-goettingen.de

Stephan Sigg, Xiaoming Fu
Computer Networks
University of Goettingen, Germany
{stephan.sigg, fu}@cs.uni-goettingen.de

ABSTRACT
Most localization systems require a physical device which is attached to the tracked object. In this project we develop an ad-hoc Device free Passive tomography and localization system. The system is ad-hoc in a sense that it does not require the exact relative location of nodes but instead learns the approximative relative topology over time. Using the Software define radio device Universal Software Radio Peripheral 1(USRP1) as a base for multiple radio links between transmitter and receiver pairs, the fundamental system works by analyzing, monitoring and processing the minimal changes in the received radio signals, to detect changes in the environment caused by moving objects. We use a movement detection algorithm to reconstruct the dynamic link graph. The scheme is derived analytically, its feasibility explored for dense networks in graphical simulations and its practicability is demonstrated in a case study with 8 nodes. The tracking algorithm reaches a localization accuracy below 1m.

Author Keywords
Indoor localization, graph topology prediction

ACM Classification Keywords
H.1.2. User/Machine Systems: Human information processing; C.3. Special-purpose and application-based systems: Signal processing systems; C.2.1. Network Architecture and Design: Wireless communication

INTRODUCTION
Indoor localization has been extensively studied and device-bound techniques have high accuracy as, for instance, demonstrated by the participants of the 2014 IPSN Indoor localization competition[1]. Device-free RF-based recognition was first investigated for the task of localization or tracking of an individual. Youssef defines this approach as Device-Free Localization (DFL) in [16] to localize or track a person using RF-Signals while the entity monitored is not required to carry an active transmitter or receiver. Popular approaches are RF-fingerprinting [6] and geometric models and estimation techniques [17]. Another approach, tomographic imaging, has been studied for several years, utilizing diverse systems such as node arrays [15], moving transmitters [8] or even passive RFID nodes [12]. The main focus of these systems is on the generation of a maximally accurate tomographic image. However, this aim demands for a high cost in terms of exact node placement and the number of nodes employed.

In this paper, we propose a system which supports random ad-hoc placement of nodes by learning the topology of the node placement.

In order to open new application cases for radio tomographic imaging, it is necessary to greatly reduce the configuration cost originating from exact relative node placement requirements. For instance, given a small number of 6–8 nodes scattered arbitrarily over the place we ask whether it is possible to obtain some (lower accuracy) tomographic image ad-hoc from those set of nodes. Our system is capable to abstract from this requirement ant do learn the topology of the network and approximate relative locations of nodes. The approach is capable of tracking location of a single moving subject with reasonable accuracy.

RELATED WORK
Tomography describes the visualization of objects via a penetrating wave. An image is then created by analyzing the received wave or its reflections from objects. A detailed introduction to obstacle mapping based on wireless measurements is given in [8, 7]. Radio tomography was, for instance, exploited by Wilson et al. in order to locate persons through walls in a room [15]. In their system, they exploit variance on the RSSI at 34 nodes that circle an area. Nodes in their system implement a simple token-passing protocol to synchronize successive transmissions of nodes. these transmitted signals are received and analyzed by the other nodes in order to generate the tomographic image, heavily relying on Kalman filters. The authors were able to distinguish a vacant area from the area with a person standing and a person moving. In addition, it was possible to identify the location of objects and to track the path taken by a person walking at moderate speed. An individual image is taken over windows of 10 seconds each. By utilizing the two-way received power fluctuations among nodes, an average localization error of 0.5 meters was reached [14].

It was reported in [1] that the localization accuracy of such a system can be greatly improved by slightly changing the

[1]http://research.microsoft.com/en-us/events/ipsn2014indoorlocalizatinocompetition/

location of sensors, thus exploiting spatial diversity. The authors present a system in which nodes are attached to disks equipped with motors in their center for rotation. With this setting it is possible to iteratively learn a best configuration (spatial location) of nodes with respect to their relative phase offset.

Wagner et al. implemented a radio tomographic imaging system with passive RFID nodes instead of sensor nodes. Implementing generally the same approach as described above, they could achieve good localization performance with their system. However, they had to implement a suitable scheduling of the probabilistically scattered transmissions of nodes in order to compensate the less controllable behavior of passive RFID [11]. In later implementations, they improved their system to allow on-line tracking [12] and a faster iterative clustering approach to further speed up the time to the first image generated [13]. This image is then of rather low accuracy but is iteratively improved in later steps of the algorithm. With this approach, it was possible to achieve a localization error of about 1.4m after only one second and reach a localization error of 0.5m after a total of about seven seconds in a 3.5m^2 area.

Utilizing moving transmit and receive nodes and compressive sensing theory [2, 3, 10] it is possible to greatly reduce the number of nodes required. For instance, Gonzalez-Ruiz et al. consider mobile robotic nodes that mount transmit and receive devices and circle the monitored target in order to generate the tomographic image [5]. In particular, they required only two moving robots attached with rotating angular antennas in order to accurately detect objects in the monitored area. Each robot takes new measurements every two centimeters. Overall, after about 10 seconds a single image can be taken. The authors detail their implemented framework in [4] and the theoretical framework for the mapping of obstacles, including occluded ones, in a robotic cooperative network, based on a small number of wireless channel measurements in [9].

In all these approaches, accurate relative location of nodes is required in order to generate the image. We will consider, instead, the generation of a tomographic image when the relative location of nodes is initially unknown to the system.

PROBLEM STATEMENT AND SYSTEM DESIGN

We consider two related problems

1. Given a known network of USRP nodes, track human movement

2. Given just the signal received at USRP receive nodes, but not the relative order of nodes, predict the topology of the USRP network based on the movement of a single human

Challenge

In this project, we assume an equal number of USRP transmit and receive nodes, which span a network of radio links with which we localize and track human movement. The individual links are identified at the receive nodes via different frequencies utilized for transmission. The receive nodes shift their center frequency every 100 μs – 500 μs to scan all channels as detailed in algorithm 1. We implement 4 baseband frequencies 899.5 MHz, 900MHz, 900.5MHz, 901MHz. The higher or lower frequency distance is degrade the USRP functionalities. For example: the higher frequency setting eliminates the frequency interference, but the delay time for frequency shifting is higher. For our real-time application, the frequency distance is optimized at 0.5 MHz. At the beginning, we create a list of feature. This set of features is the result of a feature selection and manual feature reduction we conducted on a total of 14 features and their pair-wise combination. The feature values are used as predictors for movement along each individual link.

Data: Receiving Signal S_r
Result: Receiving Power P_r
initialization;
set $f_{\max}$, $f_{\min}$;
set FFT Hamming Window size W_H= 1024;
set frequency step f_{step} = 100 kHz;
while f_r *in range (*$f_{\min}$, $f_{\max}$*)* **do**
  read current P_r;
  if $f == f_1$ **then**
    set new nearest center frequency f_c;
    $P_r = 10 * \log \sum_{i=1}^{100} S_i / \text{USRP}_{\text{rate}}$;
  else
    ;
  end
  set next center frequency $f = f + f_{\text{step}}$;
end

Algorithm 1: The algorithm to iteratively sense the radio links

Topology reconstruct step

In this phase, we will implement the motion detect between node base on the know movement route of human which interacts with the link between transmitter and receiver. The structure of the USRP node network will be observed by analyzing event in time series based.

In order to capture also simple scenarios, we assume that each node operates only as either transmitter or receiver. Let T_1 ,T_2,...,T_k be the transmit nodes and R_1,R_2,...,R_n be the receive nodes which process the captured signals. We assume a weighted undirected graph with weights $d_{ij}, i \in (1, \ldots, k), j \in (1, \ldots, m)$, for a link between T_i and R_j and weights n_{ij}^T, n_{ij}^R to represent the neighborhood relation between T_i and T_j or R_i and R_j respectively. Without loss of generality, we assume here that transmit and receive nodes are placed opposite to each other since this would be a natural choice to maximize the number of links that span the monitored area.

The purpose of our algorithm is to identify which links are intercepted by a person moving in the monitored area and to assign neighborhood relations between neighboring nodes in this graph based on the sequence in which radio links in this network are intercepted.

The weights d_{ij} and n_{ij} are initialized to 0. When a link T_i–R_j is detected to be intercepted by comparing the δ value in algorithm 2, the corresponding weight d_{ij} is set to 1. Similarly, when interception is no linger detected, it is set back to 0.

With each interception we also obtain timestamps from the USRP receive devices cf. algorithm 2. With the help of these timestamps, a sequence of interceptions is build and from which the neighborhood relations can be inferred.

Data: Receiving Power P_r
Result: Location predict base on link d_{ij}
initialization Link Array D_{ij};
while *true* **do**
  read current P_r;
  calculate $\delta = P_t - P_{t-1}$ **if** $\delta >$ *threshold* **then**
    set d_{ij}=1 $P_r = 10 * log \sum_{i=1}^{100} S_i/\text{USRP}_{\text{rate}}$;
  else
    ;
  end
  set d_{ij}=0;
end

Algorithm 2: Algorithm to update the link graph

For instance, when the link T_1–R_1 is intercepted followed by an interception of the link T_1–R_2, this is an indication that R_1 and R_2 are neighbors in the graph and the algorithm would raise its confidence on the weight n_{12}^R. Over time, all n_{ij}^R and n_{ij}^T are gradually degraded by the degrading factor $\alpha \in [0, 1[$. In practice, these sequences are significantly blurred by measurement noise but by observing these sequence of link-interceptions over a longer period of time, it is possible to build up confidence on these neighborhood relations. The actual locations are then predicted based on how many links are intercepted ($w_{ij} = 1$) and which links these are. For ease of presentation and noise reduction, we associate a Markov graph (based on the learned neighborhood relations) with distinct locations within the measurement space (cf. figure 1 for an exemplary model with 12 possible predicted locations from a 4×4 network of transmit and receive nodes).

The Markov graph contains transition arcs only between neighboring nodes. In this way, noise causing successive positive predictions of links from non-neighboring nodes can be abstracted from. The predicted state is used as a location prediction and overlayed on top of the link graph to display the predicted location on the screen.

TEST AND EVALUATION

We implement two test in different room in our Informatic faculty building, which are show in video[2]. Based on the final test result, the accuracy of the system is evaluated. When predicting the location of a moving object, some amount of noise and tracking delay must occur due to the time it takes to collect measurements from the USRP device and the program processing delays. The delay time also depends on the sampling rate and graph generation parameter, in our test the delay time is between 0.5 to 2 seconds. We test the movement through 12 known locations of a moving human are compared with the graph output. At each known location, the tracking object moves forward or backward randomly. The average estimated position location is plotted. Base on our position resolution, our error estimated 0.8 meters to 1.2 meters. Besides, our error ratio is different between each coordinate axis. In our topology, the movement which is orthogonal the link has higher accuracy than the other orients.

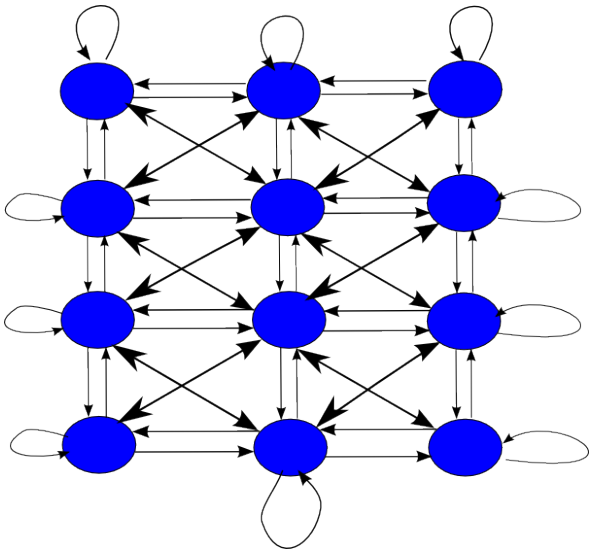

Figure 1. Markov chain with a set transition model. The choice of the future state depends only on the present state

The source code is available at: [3]

REFERENCES

1. Bocca, M., Luong, A., Patwari, N., and Schmid, T. Dial it in: Rotating rf sensors to enhance radio tomography. *arXiv preprint arXiv:1312.5480* (2013).

2. Candes, E., Romberg, J., and Tao, T. Robust uncertainty principles: exact signal reconstruction from highly incomplete frequency information. *Information Theory, IEEE Transactions on 52*, 2 (2006), 489–509.

3. Donoho, D. Compressed sensing. *Information Theory, IEEE Transactions on 52*, 4 (2006), 1289–1306.

4. Gonzalez-Ruiz, A., Ghaffarkhah, A., and Mostofi, Y. An integrated framework for obstacle mapping with see-through capabilities using laser and wireless channel measurements. *Sensors Journal, IEEE 14*, 1 (2014), 25–38.

5. Gonzalez-Ruiz, A., and Mostofi, Y. Cooperative robotic structure mapping using wireless measurements; a comparison of random and coordinated sampling patterns. *Sensors Journal, IEEE 13*, 7 (2013), 2571–2580.

[2]https://www.youtube.com/watch?v=9GeHSCogAA0&feature=youtu.be. [3]https://github.com/thachnguyen/Tomoraphy-USRP

6. Jeon, S., Suh, Y.-J., Yu, C., and Han, D. Fast and accurate wi-fi localization in large-scale indoor venues. In *Proceedings of the 10th International Conference on Mobile and Ubiquitous Systems: Computing, Networking and Services* (2013).

7. Mostofi, Y. Compressive cooperative sensing and mapping in mobile networks. *Mobile Computing, IEEE Transactions on 10*, 12 (2011), 1769–1784.

8. Mostofi, Y. Cooperative wireless-based obstacle/object mapping and see-through capabilities in robotic networks. *Mobile Computing, IEEE Transactions on 12*, 5 (2013), 817–829.

9. Mostofi, Y. Cooperative wireless-based obstacle/object mapping and see-through capabilities in robotic networks. *Mobile Computing, IEEE Transactions on 12*, 5 (2013), 817–829.

10. Needell, D., and Vershynin, R. Signal recovery from incomplete and inaccurate measurements via regularized orthogonal matching pursuit. *Selected Topics in Signal Processing, IEEE Journal of 4*, 2 (2010), 310–316.

11. Wagner, B., and Patwari, N. Passive rfid tomographic imaging for device-free user localization. In *Workshop of Positioning, NavigationCommunication* (2012).

12. Wagner, B., Striebing, B., and Timmermann, D. A system for live localization in smart environments. In *IEEE International Conference on Networking, Sensing and Control* (2013).

13. Wagner, B., and Timmermann, D. Adaptive clustering for device-free user positioning utilizing passive rfid. In *Adjunct Proceedings of the 2013 ACM International Joint Conference on Pervasive and Ubiquitous Computing (UbiComp 2013)*, UbiComp '13 (2013).

14. Wilson, J., and Patwari, N. Radio tomographic imaging with wireless networks. *IEEE Transactions on Mobile Computing 9* (2010), 621–632.

15. Wilson, J., and Patwari, N. See-through walls: Motion tracking using variance-based radio tomography. *IEEE Transactions on Mobile Computing 10*, 5 (2011), 612–621.

16. Youssef, M., Mah, M., and Agrawala, A. Challenges: Device-free passive localisation for wireless environments. In *Proceedings of the 13th annual ACM international Conference on Mobile Computing and Networking (MobiCom 2007)* (2007), 222–229.

17. Zhang, D., Liu, Y., and Ni, L. Rass: A real-time, accurate and scalable system for tracking transceiver-free objects. In *Proceedings of the 9th IEEE International Conference on Pervasive Computing and Communications (PerCom2011)* (2011).

Topological Localization with Bluetooth Low Energy in Office Buildings

Julian Lategahn, Thomas Ax, Marcel Müller, Christof Röhrig
University of Applied Sciences and Arts in Dortmund
44227 Dortmund, Germany
julian.lategahn@fh-dortmund.de

***Abstract*—Location-Based Services (LBS) require the knowledge of a user's position for manifold purposes in indoor and outdoor environments. For those applications several methods can be used, such as a Global Navigation Satellite System (GNSS). Since GNSS are not available in indoor environments or deep street canyons other techniques are required for the localization process.**

In this paper a topological map is used to implement a indoor localization system for smartphone users. Benefit of this kind of map is that the position is reduced to one dimension, which simplifies the localization process in a considerable way. The map consists of vertices, which could be important points such as crossings or a ending point of a path, and edges, which represent ways between the vertices.

The localization process utilizes different sensors of the smartphone, such as the accelerometer, bluetooth low energy and the integrated rotation vector. To combine all of these information a Extended Kalman Filter (EKF) is introduced and evaluated in an office building.

***Index Terms*—Bluetooth Low Energy; Topological Map; Pedestrian Dead Reckoning; Indoor Localization; Smartphone; Extended Kalman Filter**

I. Introduction

Localization of human operators is the basis of any Location-Based Service (LBS). LBS provide information or services with respect to the current position. There are many existing applications such as restaurant finders or museum guides, which provide information about an exhibit or lead the way to a certain point of interest.

In order to estimate a users position in a wireless system there are several techniques to accomplish this goal. An easy way to compute the position is to use the Received Signal Strength Indicator (RSSI). Most radio receivers in a wireless system have the ability to measure the strength of a signal. This signal strength can be translated to a distance by using a path loss model, as we do in this project. Another method is the use of a radio map. Here an offline phase is performed to take RSSI measurements at specified points with known positions. In the online phase the current measured RSSI values of the user are compared to the initial taken measurements. Due to this relation a user can be localized [1].

Due to the increasing demand for indoor positioning systems, wireless localization has been an important research field in the past years. In [2] a system is presented, which fuses RSSI measurements with a step detection, step length and orientation estimation. This combination increases the accuracy many times over than the stand alone usage. Similar observations were made in [3] where the authors used a combined UWB/INS System.

Due to the popularity of smartphones, which are mostly well equipped with GPS, WiFi and inertial sensors, there are many researchers working on such locating systems as presented in [4] or [5]. Also map aided approaches are very popular as the authors used in [6] or [7], where the accelerometer of a smartphone is used to detect the users steps as well as the heading and fuse this information with data from OpenStreetMap (OSM).

II. Bluetooth Low Energy Beacons

Beacons based on Bluetooth Low Energy are usually small battery-powered devices with a low power consumption and a long life cycle. They provide a broadcast which contains the identity of the transmitting beacon in a periodic time interval. It can be used for location-based advertisement, such as mobile couponing, or other LBS. Here we used the broadcasts to determine the RSSI, which is used to compute the distances between the users and the beacons.

In free space the power of a signal decreases proportional inverse quadratic to the distance between anchor and tag. In real applications this model is not applicable, because the signal is affected by several environment dependent effects. Therefor the following path loss model is often used to estimate the power of a signal $P(d^a)$ transmitted by beacon a at a given distance d^a [8]:

$$P(d^a) = P_0 - 10 n_p \log_{10}\left(\frac{d^a}{d_0}\right) \tag{1}$$

where P_0 is the signal power at a short reference distance d_0 and n_p is the path-loss exponent. In order to determine values for P_0, d_0 and n_p a series of measurements has been done. The smartphone (Google Nexus 4) was placed at different distances to a beacon, from 1 m to 30 m with a step size of 1 m. Figure 1 shows the measured RSSI values in blue and the fitted path loss model in red. It can be seen that the measurements have an inaccuracy of a few dBm, which results, due to the characteristic of the path loss model, in different distance errors depending on the real distance. As shown in figure 2 the error gains fast with the distance between smartphone and beacon.

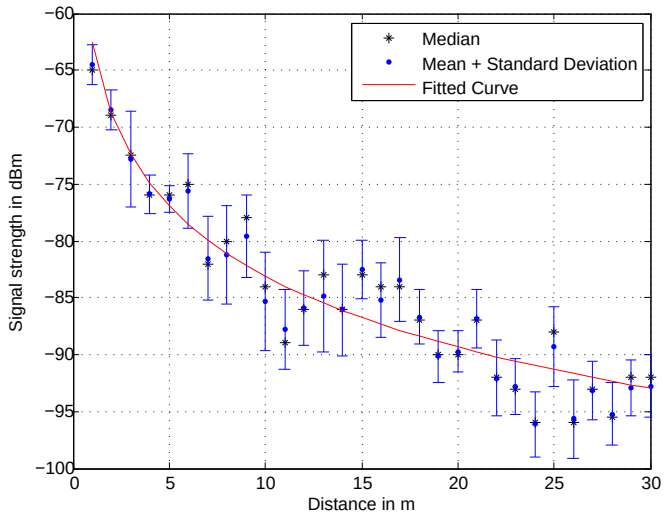

Fig. 1: Reference measurement

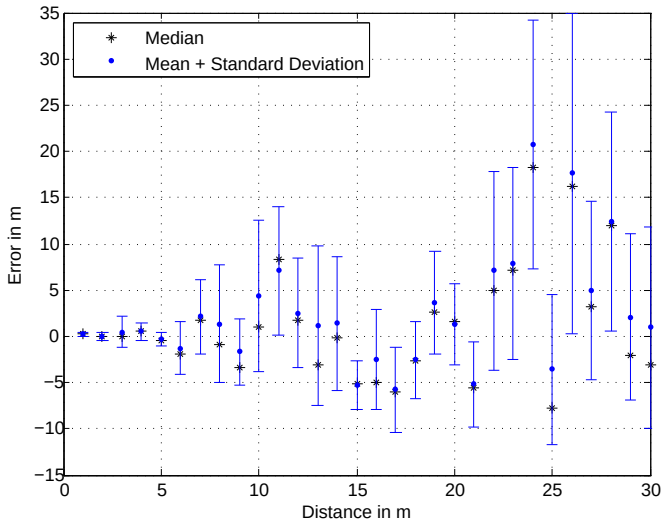

Fig. 2: Error for different distances

III. Topological Map

The topological map is one of the key features of this project. In many other applications two dimensional floor plans are used to support the localization process. But there are some disadvantages using this kind of map. The initial effort to create a map, which is usable for the localization, is fairly large and another map representation is needed for the navigation. The topological map is represented by a graph which consists of vertices and edges.

- A **vertex** is the representation of important points like crossings or doors of an office room. At those points a higher accuracy is needed for the navigation. Therefore each point is equipped with a BLE beacon.
- An **edge** represents the connection between two vertices. Every edge needs a associated distance for the localization.

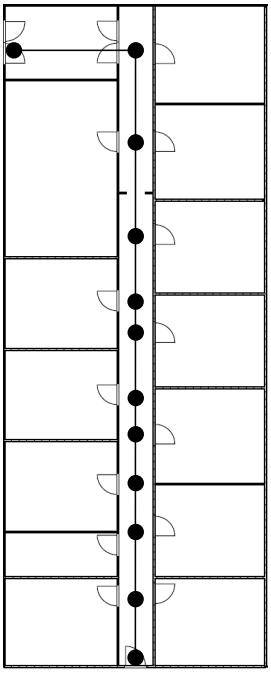

Fig. 3: Demonstration environment

Figure 3 shows our demonstration area in the computer science department at the University of Applied Sciences and Arts in Dortmund. The graph is here underlaid with the real floor plan for visualization purposes but actually it is not needed.

Another benefit while using topological maps is that the positioning process is reduced to a one dimensional problem, which is much easier to handle.

IV. Extended Kalman Filter

The Kalman Filter, which was first introduced in [9], is a recursive state estimator of a linear dynamic system. The filter handles incomplete and noisy measurement-data by minimizing the mean squared error. If the state transition or the measurement model is modeled by non-linear equations, the Extended Kalman Filter can be used instead [10]. The EKF linearizes the non-linear system by using a first order Taylor expansion. Here we used a mixed model. The state transition is a linear process with:

$$\boldsymbol{x}_k = \boldsymbol{A_{k-1}}\boldsymbol{x}_{k-1} + \boldsymbol{\omega}_k. \tag{2}$$

And the non-linear function $\boldsymbol{h}$ relates the current state to the measurement $\boldsymbol{z}_k$:

$$\boldsymbol{z}_k = \boldsymbol{h}(\boldsymbol{x}_k) + \boldsymbol{\nu}_k. \tag{3}$$

The random variables $\boldsymbol{\omega}_k$ and $\boldsymbol{\nu}_k$ represent the noise of the state transition and the measurement. They are assumed to be white, mutually independent and normally distributed with covariances $\boldsymbol{Q}_k$ and $\boldsymbol{R}_k$ respectively.

The initial position is computed by a simple algorithm. It takes the two strongest RSSI values from a five seconds measurement series into account and computes the position.

The state consists of the position on the current edge x_k and the walking speed $v_{x,k}$:

$$\boldsymbol{x}_k = \begin{bmatrix} x_k \\ v_{x,k} \end{bmatrix}. \tag{4}$$

The state transition matrix is build as follows:

$$\boldsymbol{A}_k = \begin{bmatrix} 1 & dt \\ 0 & 1 \end{bmatrix}. \tag{5}$$

The process covariance $\boldsymbol{Q}_k$ is assumed to be stable an thus it has a constant value.

A. RSSI Measurement Model

Every time a single RSSI measurement is received the EKF is performed. To use the already introduced path loss model from 1 as measurement function $\boldsymbol{h}$ in the EKF the distance d^a between the estimated user position and the a^{th} beacon has to be computed:

$$d^a = \sqrt{(x_k - x_a)^2 + (y_a)^2 + (h_a)^2}. \tag{6}$$

x_k and x_a denote the positions of the user respectively of the a^{th} beacon on the current edge. y_a and h_a are constant values and set if there is a known offset between the a^{th} beacon and the edge.

The measurement vector $\boldsymbol{z}_k^{\mathrm{RSS}}$ consists of the RSSI value of the current beacon $P(d^a)$:

$$\boldsymbol{z}_k^{\mathrm{RSS}} = P(d^a) + \boldsymbol{\nu}_k^{\mathrm{RSSI}} \tag{7}$$

In this case the measurement covariance $\boldsymbol{R}_k^{\mathrm{RSS}}$ is a constant value;

B. Velocity Measurement Model

The velocity is obtained from a step detection which utilizes the accelerometer of the smartphone. How the step detection works is already presented and explained more detailed in [11]. The measurement model of the velocity, is build quite simple:

$$\boldsymbol{z}_k^v = |v_{x,k}| + \boldsymbol{\nu}_k^v. \tag{8}$$

If there is no step detected, it is assumed that the user is not moving. So the measurement covariance $\boldsymbol{R}_k^v$ of the random variable $\boldsymbol{\nu}_k^v$ is assigned to a very small value in case of zero velocity and a higher value for non-zero velocities.

V. Experimental Results

Figure 4 shows some early experimental results of the project. Therefore we made a test walk in the already introduced office building from figure 3. The walk was made from the entry in the bottom to the end of the floor in the top and back afterwards.

A comparison between an basic EKF which uses only RSSI values and a version which combines the RSSI values with a velocity derived from a step detection is shown. The combined version shows a quiet better accuracy than the basic one.

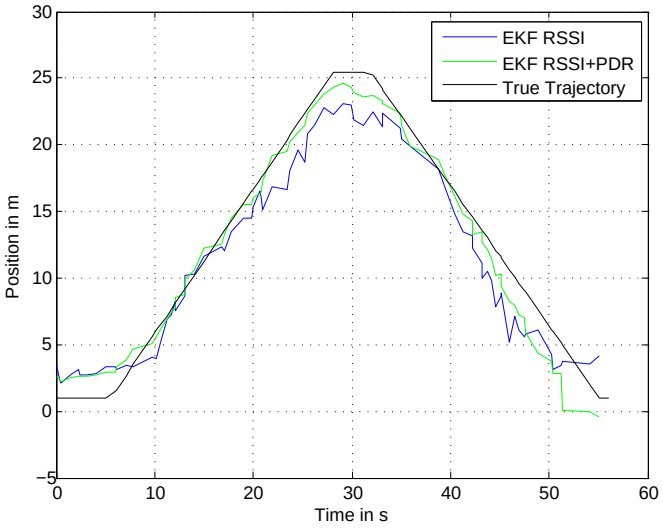

Fig. 4: 1D position on a simple test walk

References

[1] J. Tsuji, H. Kawamura, and K. Suzuki, "ZigBee based indoor localization with particle filter estimation," in *Proceedings of the 2010 IEEE International Conference on Systems Man and Cybernetics*, 2010, pp. 1115–1120.

[2] J. Schmid, M. Völker, T. Gädeke, P. Weber, and W. Stork, "An Approach to Infrastructure-Independent Person Localization with an IEEE 802.15.4 WSN," in *Proceedings of the 2010 International Conference on Indoor Positioning and Indoor Navigation (IPIN)*, 2010, pp. 1–9.

[3] S. Sczyslo, J. Schroeder, S. Galler, and T. Kaiser, "Hybrid localization using UWB and inertial sensors," *IEEE International Conference on Ultra-Wideband*, pp. 89–92, 2008.

[4] C. Lukianto, C. Hönniger, and H. Sternberg, "Pedestrian smartphone-based indoor navigation using ultra portable sensory equipment," in *Proceedings of the 2010 International Conference on Indoor Positioning and Indoor Navigation (IPIN)*, 2010, pp. 1–6.

[5] F. Hong, H. Chu, L. Wang, Y. Feng, and Z. Guo, "Pocket Mattering : Indoor Pedestrian Tracking with Commercial Smartphone," in *Proceedings of the 2012 International Conference on Indoor Positioning and Indoor Navigation (IPIN)*, no. November, 2012.

[6] Jiuchao Qian, Jiabin Ma, Rendong Ying, Peilin Liu, and Ling Pei, "An improved indoor localization method using smartphone inertial sensors," in *Proceedings of the 2013 International Conference on Indoor Positioning and Indoor Navigation (IPIN)*, 2013.

[7] J. A. B. Link, P. Smith, N. Viol, and K. Wehrle, "FootPath: Accurate map-based indoor navigation using smartphones," in *Proceedings of the 2011 International Conference on Indoor Positioning and Indoor Navigation (IPIN)*. Ieee, 2011.

[8] N. Patwari, J. Ash, S. Kyperountas, A. I. Hero, R. Moses, and N. Correal, "Locating the nodes: cooperative localization in wireless sensor networks," *Signal Processing Magazine*, vol. 22, pp. 54–69, 2005.

[9] R. E. Kalman, "A New Approach to Linear Filtering and Prediction Problems," *Transactions of the ASME - Journal of Basic Engineering*, vol. 82, no. Series D, pp. 35–45, 1960.

[10] A. H. Jazwinski, *Stochastic processes and filtering theory*. New York: Academic Press, 1970.

[11] J. Lategahn, M. Müller, and C. Röhrig, "Robust Pedestrian Localization in Indoor Environments with an IMU Aided TDoA System," in *Proceedings of the 2014 International Conference on Indoor Positioning and Indoor Navigation (IPIN 2014)*, Busan, Korea, 2014.

Clustering of Inertial Indoor Positioning Data

Lorenz Schauer and Martin Werner
Mobile and Distributed Systems Group
Ludwig-Maximilians Universität, Munich, Germany
lorenz.schauer@ifi.lmu.de, martin.werner@ifi.lmu.de

***Abstract*—TRACLUS is a widely-used partitioning and grouping framework for trajectories. However, suitable clustering results representing the building's topologies are hardly obtained when applying the framework to indoor trajectories with noise. In this work, this problem is demonstrated on an inertial indoor positioning data set created using a filtered dead-reckoning system based on step-counting. Using Douglas-Peucker algorithm as a different segmentation strategy to TRACLUS and a minor correction to the distance weightings of TRACLUS, we show that this framework is still applicable for this data set.**

***Keywords*-Indoor Trajectories; Segmentation; Density Clustering; TRACLUS**

I. Introduction

In the last decade, modern mobile devices with integrated sensors have generated new possibilities and challenges for indoor localization and tracking. More and more location data from mobile users is becoming available and has to be processed with the methods of data science, such as trajectory clustering algorithms, in order to understand and use this valuable personal information. This topic is of high interest for many fields in the scientific and commercial world. We see an important application domain in filtering of noise and uncertainty in indoor positioning systems without map information: the clustering structure of trajectories creates a valuable "map", which can be used to assess the probability location in particle filtering or multiple-hypothesis tracking navigation approaches.

In this work, we focus on a well-known and widely-used trajectory clustering framework and algorithm named TRACLUS [1] and show its deficits for a real-world inertial indoor positioning data set. We demonstrate, how these deficits can be solved with minimal changes of the proposed framework. Using Douglas-Peucker algorithm [2] as another segmentation strategy, and a slightly up-weighted angle distance, we receive more adequate clustering results representing the topology of the corresponding building.

The remainder of the paper is organized as follows: The next Section II shortly introduces the TRACLUS frameworks and the relevant definitions. In Section III, we first describe the used dataset, its internal structure, and the results of the original TRACLUS algorithm. Then, we show that a different segmentation leads to the expected results. Finally, Section IV concludes the paper.

II. The TRACLUS algorithm

The TRACLUS algorithm [1] is a widely-used partitioning and clustering framework performing density-based clustering on line segments, rather than grouping trajectories as a whole. This is due to the fact that capturing the distance between non-local objects is infeasible and, therefore, some locality is reconstructed by a splitting methodology. In order to get line segments, the trajectory is partitioned on segmentation points representing significant changes of the trajectory's behavior. Hence, as a first step, segmentation points have to be found. For trajectory segmentation, several approaches have been presented in literature [2]–[4]. TRACLUS performs an approximate solution based on the minimum description length (MDL) principle in order to find the optimal tradeoff between preciseness and conciseness.

In a second step, the line segments from the partitioning phase are clustered with respect to their density-connectedness. Different density-based clustering algorithms can be found in literature such as DBSCAN [5] or DENCLUE [6]. TRACLUS is similar to DBSCAN and searches density-connected sets of line segments which are marked as clusters. As in case of DBSCAN, two parameters are required: ϵ defining the threshold for the ϵ-neighborhood of line segments, and *minLns*, defining the minimum amount of lines which have to be inside an ϵ-neighborhood in order to create a cluster.

In order to compute the ϵ-neighborhood of a line segment, a distance function is needed focusing on segment characteristics. TRACLUS proposes three distances capturing different aspects of similarity: parallel distance (PD), perpendicular distance (PPD), and angle distance (AD). These are joined into a single distance measure by a weighted sum, with weight $\alpha_i = 1$ by default:

$$d = \alpha_1 PD + \alpha_2 PPD + \alpha_3 AD$$

In a final step, all clusters are checked if their trajectory cardinality is greater that a predefined threshold which is *minLns* by default. Otherwise they are removed from the result set of clusters. This is done, because a cluster of segments coming from a small set of trajectories could lead to a cluster of trajectories containing less than *minLns* individual trajectories.

III. Clustering of Inertial Indoor Positioning Data

In order to extract reasonable map information from inertial sensor systems, this section proposes to use a blind clustering approach without any map information and demonstrate its feasibility on a real-life dataset.

A. The Dataset

Using a dead-reckoning system based on step counting and a digital compass, we created several traces inside our building which are depicted in Figure 1(a). For reference, Figure 1(b) depicts the schematic floor plan of the building. The dataset consists of a user walking into each of the hallways, turning there and walking back. It suffers from accumulating errors as there are no reference measurements integrated into the system, however, the used sensory and filtering led to quite accurate results as can be seen. The dataset consists of 10 trajectories for a total of 10,386 step estimates of varying length and direction.

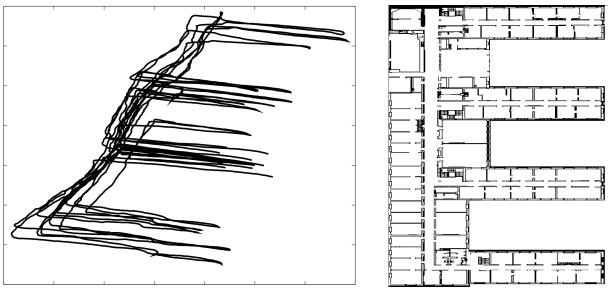

(a) Representation of data set (b) Schematic floor plan

Figure 1. Data set created within our office building

Using this dataset, we would expect to find four clusters representing the horizontal hallways and either one or three clusters representing the vertical interconnections between them. We expected this as the trajectories in these clusters would have been similar to each other in direction and length as well as near to each other while they would not be near to trajectory parts in other hallways.

B. TRACLUS Results

For clustering, we used TRACLUS in two different fashions: First, we perform segmentation and distance weightings as proposed in the original publication.

Performing this with a value of *minLns* $= 3$, we varied the parameter ϵ and were unable to produce the expected results: For large values of ϵ, of course, too few clusters were detected. For smaller values, however, some of the clusters broke up into two different ones and clusters got rejected based on that they did not meet the *minLns* threshold anymore rendering those candidates as noise. Figure 2 depicts a situation for $\epsilon = 1.8$. While some clusters start breaking wrongly into two different clusters (low part of Figure 2(b)), highly unrelated clusters are being joined such as the T-shaped cluster in the middle. This is due to problems with the segmentation and especially with short segments therein, see Figure 2(a). These short segments are taken as similar with each other by the original TRACLUS construction [1].

It is clear from this figure, that no other value of ϵ would have created the expected results: smaller values increase the splitting of relevant clusters, larger values will not lead to a breakup of the T-shaped cluster. Consequently, we have to change the algorithm in another way.

From Figure 2(a), we observe that the MDL-based segmentation of TRACLUS results in very small segments which actually do not capture any trend change in their definitions. In order to change that, we decided to use the Douglas-Peucker line simplification algorithm in order to capture a segmentation of the input trajectories which is less sensitive to small perturbations. As you can see in Figure 3(a), the Douglas-Peucker simplification rejects more points as compared to the original TRACLUS segmentation. Furthermore, it keeps those points where durable changes in orientation actually take place. As a first effect, this reduces the computational overhead. More importantly, however, the clusters capture more information: The line segments that we expect to fall into same clusters not only have similar orientation, but have similar length and some nearness of endpoints. In order to get a distance measure sensitive to the differences in angles between those segments and not overemphasizing the nearness of completely parallel segments of similar length, we had to change the weighting in the original TRACLUS distances towards angle distance. Note that executing the original TRACLUS with these modified weightings led to an even worse clustering result, as a lot of non-related segments have similar orientation. Using Douglas-Peucker segmentation, however, the result of clustering with modified weightings is depicted in Figure 3(b). This result finds all clusters as expected without the topmost cluster, which is anyways underrepresented in the dataset and correctly removed, due to its low trajectory cardinality.

In summary, we showed that the TRACLUS framework is still applicable to inertial indoor trajectories. However, the TRACLUS segmentation is too sensitive to measurement variations. We changed the segmentation as well as the distance weightings such that the intuitive notion of a cluster in the given dataset is actually reached.

Note that we did not yet show that this approach is generally advantageous for indoor trajectories. Still, we provide an example and an approach, which is tailored to the nature of inertial trajectories. Therefore, we expect that this approach will be applicable to other datasets in which measurement perturbations would lead to short segments as well as in which large segments can be extracted, which capture the actual structure of the dataset.

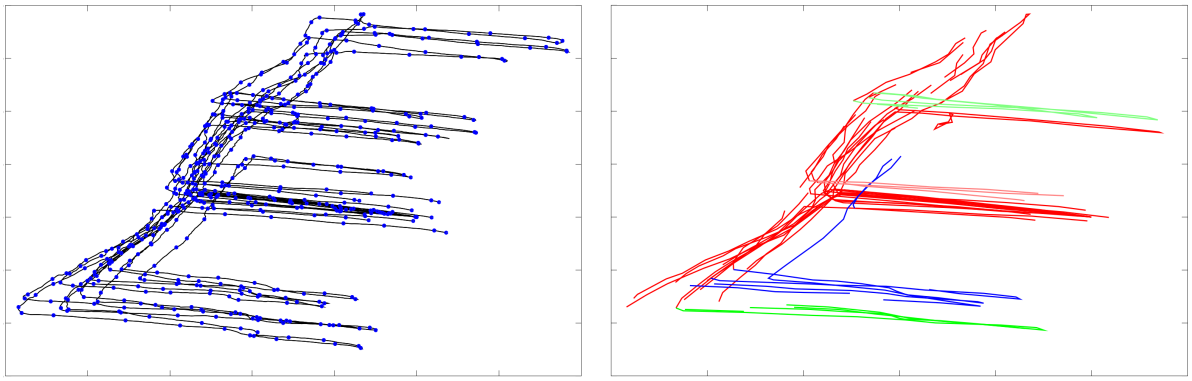

(a) TRACLUS segmentation result

(b) TRACLUS clustering result with $\epsilon = 1.8$

Figure 2. Results of using TRACLUS in its original form on inertial tracking data.

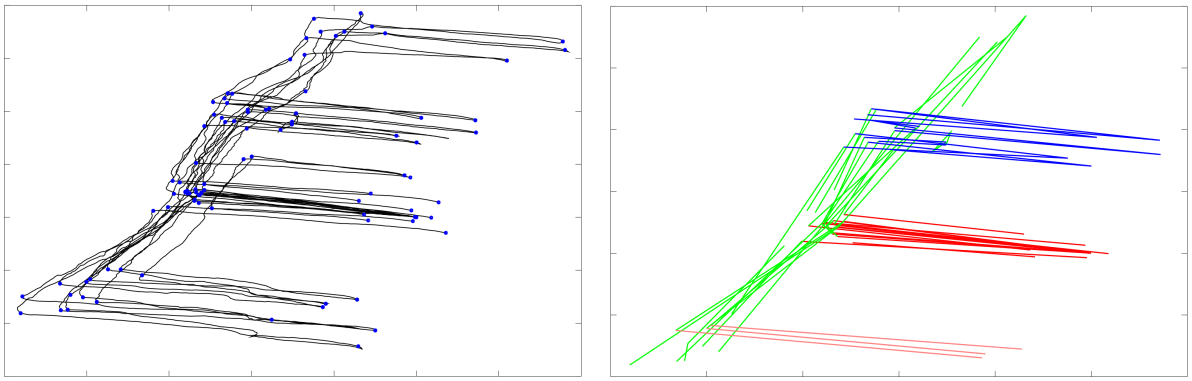

(a) Douglas-Peucker segmentation

(b) TRACLUS using Douglas-Peucker ($\epsilon_{\text{DP}} = 2$), modified distance weight ($\alpha_3 = 2$), and $\epsilon = 6$

Figure 3. Results of using Douglas-Peucker for segmentation together with TRACLUS clustering on inertial tracking data.

IV. Conclusion and Future Work

In this work, we have addressed the problem of clustering inertial indoor positioning data. We have shown that the widely-used TRACLUS algorithm in its original form does not fit to this problem. Furthermore, we have demonstrated that the clustering results not only depend on both parameters ϵ and *minLns*, but also on the used segmentation strategy. Replacing the TRACLUS segmentation with Douglas-Peucker, the clustering results became more adequate for our purpose.

For future work, we want to enhance our investigations using different parameters and a large number of indoor data sets. We plan to use various distances for trajectories in order to compute the ϵ-neighborhood and evaluate the quality of returned clusters by using well-known quality measures for clustering as well as novel application-centered measures which capture the special situation inside buildings and other complex surroundings.

References

[1] J.-G. Lee, J. Han, and K.-Y. Whang, "Trajectory clustering: a partition-and-group framework," in *Proceedings of the 2007 ACM SIGMOD international conference on Management of data*. ACM, 2007, pp. 593–604.

[2] D. H. Douglas and T. K. Peucker, "Algorithms for the reduction of the number of points required to represent a digitized line or its caricature," *Cartographica: The International Journal for Geographic Information and Geovisualization*, vol. 10, no. 2, pp. 112–122, 1973.

[3] M. Potamias, K. Patroumpas, and T. Sellis, "Sampling trajectory streams with spatiotemporal criteria," in *Scientific and Statistical Database Management, 2006. 18th International Conference on*. IEEE, 2006, pp. 275–284.

[4] P. Katsikouli, R. Sarkar, and J. Gao, "Persistence based online signal and trajectory simplification for mobile devices," 2014.

[5] M. Ester, H.-P. Kriegel, J. Sander, and X. Xu, "A density-based algorithm for discovering clusters in large spatial databases with noise." in *Kdd*, vol. 96, 1996, pp. 226–231.

[6] A. Hinneburg and H.-H. Gabriel, "Denclue 2.0: Fast clustering based on kernel density estimation," in *Advances in Intelligent Data Analysis VII*. Springer, 2007, pp. 70–80.

Lane-Level Localization on Lanelet Maps Using Production Vehicle Sensors

Johannes Rabe, Sascha Quell, Marc Necker
Research and Development
Daimler AG
Sindelfingen, Germany
{johannes.rabe, sascha.quell, marc.necker}@daimler.com

Christoph Stiller
Institute of Measurement and Control
Karlsruhe Institute of Technology
Karlsruhe, Germany
stiller@kit.edu

***Abstract*—An approach for localization for lane-accurate navigation systems is proposed. The method uses a particle filter to determine the ego-vehicle's lane and the lateral and longitudinal position within this lane on a lanelet map. As inputs a visual sensor for lane-marking detection, radar information on moving objects in the surroundings, the digital map, yaw rate, and odometry – all available in a current production vehicle – are used. The algorithm has proven successful in tests in over 97% of the time.**

I. Introduction

Imagine you are driving your car somewhere you have never been before and find yourself in this situation: You exit a roundabout, the road immediately splits into five lanes and you are supposed to turn left at the next intersection as outlined in Fig. 1. Future navigation systems shall help you in this situation and provide lane-level maneuver advise. They shall not only inform about the optimal lane leading to your destination, but also propose lane changes that might be required. For this purpose, it is of course necessary to robustly determine the current lane of the ego-vehicle in any situation.

The most crucial point is in front of complex intersections where accurate lane advise is most beneficial. Furthermore, determining the ego-lane with acceptable accuracy on highways after traveling several kilometers and performing a couple of lane changes is a doable task. Trying the same in city roads and in situations like the one introduced in Fig. 1, however, can quickly become more difficult.

So far, there has been a lot of research on accurate localization of vehicles, especially in the context of advanced driver assistance systems and automated driving. Many publications use special maps containing landmarks collected by cameras, lidar or radar sensors [1], [2], [3]. However, this approach is currently not feasible for the purpose of a navigation system that shall be able to work on most roads of the network.

In our approach, we use abstract data from a camera and radar sensors available in a current production Mercedes-Benz S-Class as well as a lanelet map [4]. This data is fused with a particle filter yielding an estimate for the currently driven lane as well as the lateral and longitudinal position in this lane. The combination of radar and camera data allows for positioning both in cases of heavy traffic, where lane markings may be hidden behind other vehicles, as well as in cases of low traffic, where the positioning relative to other vehicles is limited.

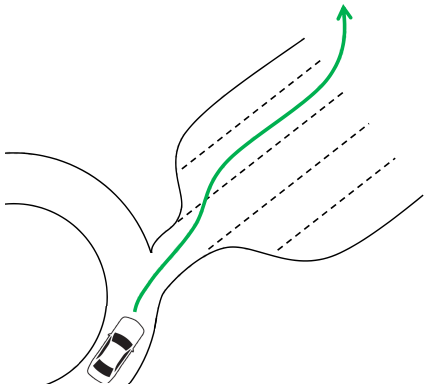

Fig. 1. Lane-level navigation advising the driver to take the fourth lane to turn left after exiting a roundabout. The green line shows a possible route.

After an overview over related work, the following Section III describes the basic properties sensors and data used in the particle filter. Section IV presents the actual sensor fusion process. Exemplary results are provided in Section V before a conclusion and outlook on further work is given in Section VI.

II. Related Work

A couple of different approaches for the determination of the ego-lane have been proposed in previous work. In [5], a particle filter method for ego-localization on a precise digital map is presented. The measurement model includes absolute positioning with a low cost GPS, a highly precise map and the position and orientation angle of the ego-vehicle in its lane as computed by image analysis. The system state contains the vehicle's coordinates in reference to the map and its orientation angle.

A similar approach is followed by [6]. However, the estimated system state consists of link and lane id of a map and the offset relative to the beginning of the link. The vision sensor tracks the distances to the next lane-markings on the left and right side as well as their types.

In [7], an algorithm based solely on vision is presented. Spatial ray features are used to analyze the layout of the road

scene to determine the number of lanes to the left and right of the ego-vehicle.

The approach shown in [8] is even capable of exact positioning in small city streets without lane-markings. However, a laser-scanner is required for measuring street and building structures in the environment of the vehicle which is currently neither state-of-the-art in production vehicles and nor is it expected in the near future due to its prohibitive costs.

III. Sensors

For the localization algorithm, mainly the three sensors described in the following are used.

A. Lanelet Map

Lanelet maps were originally proposed in [4] in the context of automated driving. These maps contain geometrical and topological properties of the road network. Every lane and driving option is stored as a "lanelet", geometrically described by its left and right boundary. As every lanelet shares nodes with its predecessor and successor, the geometrical representation can be converted into a graph containing the topological information and allowing for routing through the network.

The map used in this work was hand-made in the JOSM editor based on Bing satellite images. To allow for an evaluation of the estimated ego-lane in comparison to a ground truth ego-lane, we added an initialization step to find neighboring lanes and enumerate the road segments.

B. Lane Marking Detection

A stereo camera mounted behind the windshield and computer vision algorithms allow for detection of lane markings in front of the vehicle. The information provided contains, among others, the distance to the closest marking on the left and right side of the camera, its type (continuous, dashed, ...), and the yaw difference between the vehicle coordinate system and the detected marking.

C. Moving Radar Objects

In case of obstructed sight due to heavy traffic in front of the vehicle, fewer lane markings can be detected. Therefore, information from a front radar about moving objects in front of the ego-vehicle is used. For each moving object, the relative position x_v and y_v in vehicle coordinates and an estimate for its type (car, truck, ...) is provided. With this data, the ego-vehicle localization can be supported: If there are vehicles moving in a similar direction as the ego-vehicle two lanes left of the ego-vehicle, it is quite likely that the ego-vehicle is not on one of the two leftmost lanes. The same holds accordingly for other detected positions.

IV. Sensor Data Fusion

The localization algorithm fuses the signals from the aforementioned sensors using a particle filter. It estimates the posterior density of the system state $\mathbf{x}_k$ at time k given the sensor measurements $\mathbf{z}_0, \ldots, \mathbf{z}_k$ up to the current time step, $p\left(\mathbf{x}_k | \mathbf{z}_0, \ldots, \mathbf{z}_k\right)$. For this a motion and measurement model as described in the following are used. The system state consists of the vehicle position in two dimensions and its corresponding heading angle. This leads to a three-dimensional state vector $\mathbf{x}_k = (x_k, y_k, \psi_k)$, where x_k and y_k refer to the East and North component of a local East-North-Up (ENU) frame, respectively, and ψ_k to the heading angle in the East-North-plane.

The particle filter is initialized based on a GPS fix containing latitude and longitude in a World Geodetic System 1984 (WGS-84) coordinate frame and an estimate for the heading since the previous GPS fix. The particles' 2D position and their heading are drawn randomly from a normal distribution around this GPS position.

To avoid degenerate sets of particles, the particles are periodically resampled according to their original accumulated weight [9].

A. Motion Model

The motion model for the prediction step is based on wheel odometry sensors and a yaw rate sensor. The vehicle is modeled as a point in space that rotates according to the measured yaw rate and always moves straight forward into its heading direction. This model has shown to be reasonable in comparisons with alternative motion models.

B. Measurement Model

In the update step, the observations from the sensors mentioned in Section III are used to assign weights to the set of particles.

1) Digital Map: For the digital map weight, the pseudo-distances of each particle to the left and right borders of lanelets in its near environment are determined as described in [4]. Based on these pseudo-distances, on-road lanelets can be assigned to lanelets. The weight for particles i which couldn't be assigned to any lanelet is set to a minimum value $w_{\mathrm{map},i} = w_{\mathrm{map,min}}$. For each on-road particle, the weight is calculated from the difference in heading $\Delta\psi_i$ between the mean pseudo-tangent at its position on the lanelet and the particle heading ψ_i but lower bounded by the same minimum value that is assigned to off-road particles:

$$w_{\mathrm{map},i} = \max\left(\cos\left(\Delta\psi_i\right), w_{\mathrm{map,min}}\right). \tag{1}$$

2) Type of Lane-Marking: For the particle weight based on the detected lane-marking type, we assume a highway-like road marking with continuous lines on the outer boundaries of a road and dashed or similar not continuous lines between adjacent lanes of one road. The markings on both sides are treated independently and depend on the lanelet that a particle has been assigned to in the digital map weight step. For example, a dashed left marking leads to a reduced weight for particles on the leftmost lane, whereas particles on all other lanes get assigned a higher weight.

3) Distance to Lane-Marking: Apart from the marking type, also the distance to the road marking plays a role. For this purpose, the pseudo-distance to the left or right boundary of the lanelet estimated during the lanelet weight is compared to

the distance to the respective marking detected by the camera. The difference Δd_i between both leads to a weight

$$w_{\mathrm{md},i} = \max\left(\left\{\exp\left(-\frac{(\Delta d_i)^2}{2\sigma^2}\right), w_{\mathrm{md,min}}\right\}\right) \quad (2)$$

for particle i, where the standard deviation σ depends on the confidence level of the lane marking detection algorithm. A special treatment is performed for cases where the detected lane-marking might be ambiguous.

4) Moving Radar Objects: The fourth component of the update step is the weight based on the objects detected by the front radar. For this purpose, moving objects classified as cars or trucks are projected onto the map based on their estimated relative position and the heading and position of each particle. The resulting point in space is then in turn tested whether it lies upon a road in the digital map. Depending on this mapping, a higher or lower weight is applied.

V. Preliminary Results

The proposed algorithm has been tested in a simulation environment on different roads. Over a test set of around 12 minutes of roads in city and rural roads with up to five lanes, the algorithm has estimated the correct lane in 97.5% of the time.

However, any test track may contain single-lane segments or long parts without turns that make the estimation easier, as well as traffic lights which lead to distorted time measurements. Therefore, the mere percentage of correct estimates over time or distance is not the most meaningful performance measure for an inner-city ego-lane estimation and we are currently working on an improved measure as well as a proper data set. This shall take into account that the problem becomes easier on single lanes and with frequent lane changes, but also that the estimation is most crucial in the approach of a complex intersection.

So long, we want to show exemplarily how the algorithm handles the situation shown in Fig. 1. The roundabout is shown at the bottom left corner of Fig. 2 and left by the vehicle toward the five lane road. The particle filter correctly determines the fourth lane as the most likely hypothesis with some particles remaining as concurrent hypotheses on the third and second lane.

As has already been found in [6], the observation of the distance to the detected road markings is very helpful as it allows for an easy detection of lane changes.

VI. Conclusion and Outlook

We have presented a method for lane-level localization of a current production vehicle using sensors available ex works, namely vision, radar, yaw rate, and wheel odometry, and a digital map. The algorithm is capable of determining the current lane of the ego-vehicle in many cases based on lane-marking detection and other traffic, even without a certain number of lane changes required between initialization and the first stable lane estimate.

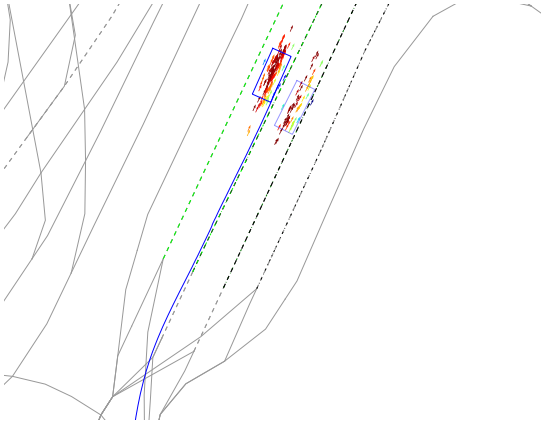

Fig. 2. Localization result on five lane road. The weighted average position with respect to the lane as blue boxes and history of the overall average as a blue line. The estimated lanelets are highlighted in green.

Future work will contain the production of a proper data set as well as the determination of a useful performance measure. We will also compare the influence of the different sensors used on the overall result as well as different weighting of separate sensors. A next step is the use of an actual commercial map on roads where it is available in reasonable detail as well as the examination of the influence of missing or wrong information on the result. The behavior over very long distances on more or less straight roads has yet to be evaluated.

References

[1] J. Ziegler, P. Bender, M. Schreiber, H. Lategahn, T. Strauss, C. Stiller, T. Dang, U. Franke, N. Appenrodt, C. G. Keller, E. Kaus, R. G. Herrtwich, C. Rabe, D. Pfeiffer, F. Lindner, F. Stein, F. Erbs, M. Enzweiler, C. Knöppel, J. Hipp, M. Haueis, M. Trepte, C. Brenk, A. Tamke, M. Ghanaat, M. Braun, A. Joos, H. Fritz, H. Mock, M. Hein, and E. Zeeb, "Making Bertha Drive–An Autonomous Journey on a Historic Route," *IEEE Intelligent Transportation Systems Magazine*, vol. 6, no. 2, pp. 8–20, 2014.

[2] C. Tessier, C. Debain, R. Chapuis, and F. Chausse, "Simultaneous landmarks detection and data association in noisy environment for map aided localization," in *Intelligent Robots and Systems, 2007. IROS 2007. IEEE/RSJ International Conference on*. IEEE, 2007, pp. 1396–1401.

[3] H. Lategahn and C. Stiller, "City GPS using stereo vision," in *Vehicular Electronics and Safety (ICVES), 2012 IEEE International Conference on*. IEEE, 2012, pp. 1–6.

[4] P. Bender, J. Ziegler, and C. Stiller, "Lanelets: Efficient Map Representation for Autonomous Driving," in *The 25th IEEE Intelligent Vehicles Symposium*, Dearborn, Michigan, USA, Jun. 2014.

[5] F. Chausse, J. Laneurit, and R. Chapuis, "Vehicle localization on a digital map using particles filtering," in *Intelligent Vehicles Symposium, 2005. Proceedings. IEEE*. IEEE, 2005, pp. 243–248.

[6] I. Szottka, "Particle filtering for lane-level map-matching at road bifurcations," in *Intelligent Transportation Systems, ITSC. IEEE International Conference on*, 2013, pp. 154–159.

[7] T. Kühnl, F. Kummert, and J. Fritsch, "Visual ego-vehicle lane assignment using spatial ray features," in *Intelligent Vehicles Symposium (IV), 2013 IEEE*. IEEE, 2013, pp. 1101–1106.

[8] R. Matthaei, G. Bagschik, and M. Maurer, "Map-Relative Localization in Lane-Level Maps for ADAS and Autonomous Driving," in *The 25th IEEE Intelligent Vehicles Symposium*. Dearborn, Michigan, USA: IEEE, Jun. 2014.

[9] Z. Chen, "Bayesian filtering: From Kalman filters to particle filters, and beyond," *Statistics*, vol. 182, no. 1, pp. 1–69, 2003.

Testbed for automotive indoor localization

Daniel Becker[1], Fabian Thiele[1], Oliver Sawade[2], Ilja Radusch[2]

***Abstract*— To enable intelligent vehicular indoor applications highly accurate localization is required. There is a high number of different approaches which are however difficult to compare due to a lack of a common evaluation methodology. Thus, we present a testbed for vehicular indoor localization, to enable the benchmarking of different approaches under comparable conditions. As a first building block, we present a simple yet highly accurate ground truth system based on off-the-shelf infrastructure cameras and printable markers. Our employed marker detection algorithm and systematic 3-layer projection approach achieves a median accuracy of 0.48cm and 0.05 degrees for 2D position and orientation.**

I. Introduction

There are countless applications for vehicles operating indoors, ranging from intelligent vehicles to industrial robots and automated warehouses. Requirements in terms of localization accuracy and reliability tend to correlate with the degree of automation. Especially for completely automated systems (i.e. operating without human supervision), localization requirements are particularly high.

In recent years, intelligent and automated vehicles for indoor carparks have attracted a significant attention of the research community as these systems have the potential to alleviate congestion problems in modern cities. One of the core technologies to enable this vision of indoor automated driving is highly accurate localization. To achieve it, a multitude of different localization approaches based on various technologies (e.g. cameras, laser scanners, odometry, etc.) can be applied [1] [2] [3]. However, the performance of these systems is often condensed into a few numerical values for the median, standard deviation, minimum, maximum error or quantiles of the localization accuracy. Nevertheless, the comparison of different techniques based on these metrics is often difficult as they are not clearly defined and testing conditions vary significantly. Thus, the necessity for a vehicular indoor testbed arises, in order to benchmark different localization techniques in identical conditions [4] [5].

Our goal is to develop a testbed for automotive indoor localization techniques in parking scenarios. One essential building block for a testbed is a *Ground Truth* system, i.e. a localization system that is highly accurate and robust, ideally surpassing the desired localization accuracy of the productive system by an order of magnitude. In particular for the task of automated driving in indoor carparks, an accuracy of at least 10cm and 1° for position and orientation is commonly quoted as sufficient [1] [2]. Thus, an accuracy of at least 1cm and 0.1° would be ideal for the Ground Truth system.

Outdoors, GNSS based systems are often used as Ground Truth. A common variant is DGPS (Differential GPS) where the accuracy is improved by adding stationary transponders at fixed known locations. Under typical outdoor conditions, 1m localization accuracy can be achieved [4]. However, in indoor spaces or other conditions without line-of-sight to the navigation satellites, the accuracy of GNSS systems decreases or ceases entirely [4].

In this work, we present a highly accurate yet cost-effective Ground Truth system based on customary infrastructure cameras and printable optical markers forming an important building block of our automotive indoor testbed.

II. Methodology

The backbone of the proposed Ground Truth approach is a reference grid with a chessboard pattern and a camera facing down onto the grid, as shown in Fig. 1. This figure shows the placement of the reference grid in our testbed [3] and the coverage of the camera onto the grid (indicated in blue). The grid consists of alternating black/white square shapes with a side length of 16.4cm. The camera is at a mounting

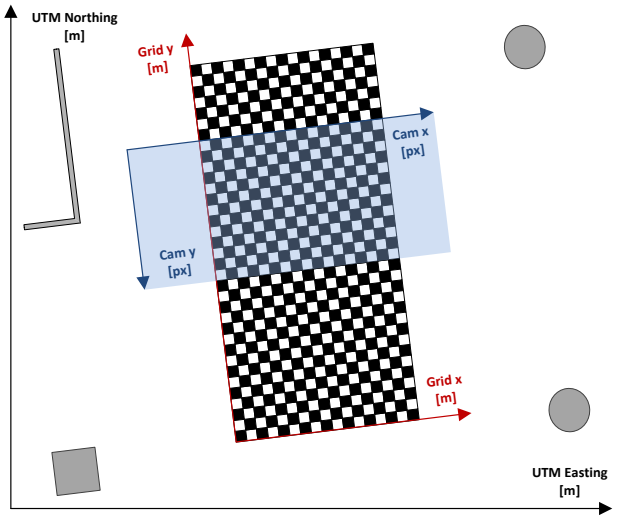

Fig. 1: Reference chessboard grid and camera view in indoor carpark environment, showing camera (blue), reference grid (red) and global UTM (black) coordinate systems.

[1]Daniel Becker and Fabian Thiele are with the Daimler Center for Automotive Information Technology Innovations (DCAITI), Ernst-Reuter-Platz 7, 10587 Berlin, Germany {daniel.becker,fabian.thiele}@dcaiti.com

[2]Oliver Sawade and Ilja Radusch are with the Fraunhofer Institute for Open Communication Technologies (FOKUS), Kaiserin-Augusta-Allee 31, 10589 Berlin, Germany {oliver.sawade,ilja.radusch}@fokus.fraunhofer.de

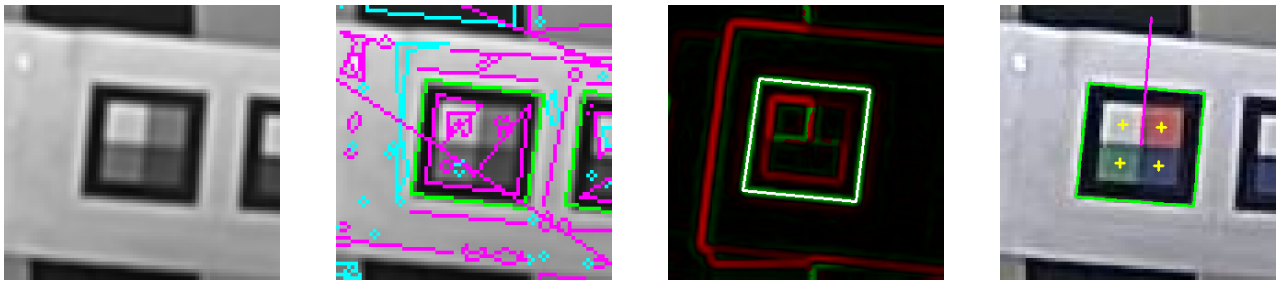

(a) Prepocessed input image (b) Detected contours (c) Edge refinement (d) Marker ID sampling

Fig. 2: Image processing steps of the marker detection algorithm.

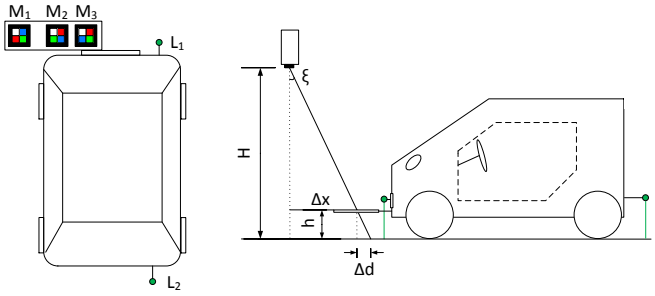

Fig. 3: Test vehicle equipped with color markers and reference laser pointers, top view (left) and side view (right).

height H (cf. Fig. 3) of 2.75m and its view covers a total area of 2.1m x 3.4m. Also, 4 map objects are shown in Fig. 1 (1 wall, 1 square pillar and 2 round pillars). These map objects are represented in a given indoor map with geographic coordinates (UTM [6]). Thus, each map object is located on 3 coordinate systems: 1. global (e.g. UTM in meters) 2. reference grid (in meters) 3. camera view (in pixels). Multiple grids and cameras are possible but for simplicity's sake we assume there is only one of each.

The goal of the presented approach is to automatically detect objects in the camera view and project the position into the reference grid as well as global coordinate system - as accurately as possible. We developed a detection algorithm for printable squared colored markers as shown in Fig. 2. This algorithm consists of multiple steps, including preprocessing of the image, detecting of the approximate contours, edge refinement using grayscale gradients and sampling of a unique ID based on the color pattern. As a result, this algorithm yields the central position in the camera view (in pixels) as well as a unique identifier (max 32 combinations).

In the second step, the camera view position (pixels) is projected onto the reference grid (meters) by utilizing a homography projection matrix obtained during an initial calibration process for each camera image. The calibration process utilizes two sets of corresponding camera view and reference plane positions (i.e. chessboard corners, cf. Fig. 1) and determines a projection matrix H_A by utilizing OpenCV function cvFindHomography() [7]. H_A describes 2 rotations and 1 translation and can be multiplied with a camera view position to yield the corresponding reference plane position.

The third and last step is the determination of the global position (e.g. UTM projection [6] coordinate in meters) which is done similarly to the projection step between camera view and reference grid. The required two sets of corresponding points are generated from known characteristic positions of structural elements (e.g. corners, pillars) where both the global and reference grid coordinate is known. Thus, OpenCV function cvFindHomography() [7] can be applied and yields a projection matrix H_B, able to convert reference grid to global coordinates and vice versa.

III. Evaluation

We equipped our underground carpark test site [3] with *AXIS Q1604 (FW: 5.40.3.1)* network cameras at mounting heights of 2.75m which provide MJPEG encoded images at 24fps and a resolution of 1280x720px via Gigabit Ethernet. A Smart Fortwo acts as test vehicle equipped with markers at a mounting height of 0.23m. The software is written in C++ making use of the library OpenCV 2.4.9 and runs on a computer with Intel(R) Core(TM) i7-4700MQ and 16GB RAM with Ubuntu 12.04 LTS (64 bit).

A. Overall Positioning Error

As shown in Fig. 3, we attached two laser pointers to the test vehicle which project a point onto the grid that can be measured manually. Assuming the manual measurements are done at an accuracy of at least 1mm is sufficient as reference position for evaluating our proposed approach.

As the mounting of markers and laser pointers is rigid, the displacement is constant over time. To be able to compare marker position $p_{ref,M}$ and manually measured position $p_{ref,L1}$, we perform a shift to the vehicle reference point:

$$p_{ref,V} \mathrel{\widehat{=}} p_{ref,L1} \mathrel{\widehat{=}} p^{\triangleright}_{ref,M} \tag{1}$$

Consequently, we define the error in terms of position as:

$$E_{pos} = |p_{ref,V} - p^{\triangleright}_{ref,M}| \tag{2}$$

Also, the error for the orientation angle is defined as:

$$E_{\theta} = |\theta_{ref,L} - \theta_{ref,M}| \tag{3}$$

In order to determine the overall positioning error, the vehicle was placed at 15 different positions in the camera view, i.e. variations in $p_{ref,V}$ and $\theta_{ref,L}$.

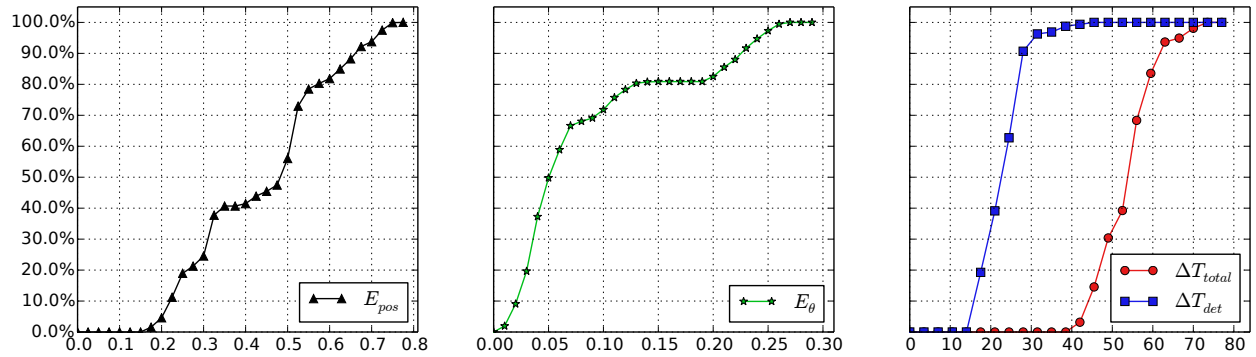

Fig. 4: Evaluation results, Cumulative Density Functions (CDF) of A) position error E_{pos} in cm, B) orientation error E_θ in $^\circ$ and C) detection time ΔT_{det} and total time ΔT_{total} in ms.

Fig. 4 A) displays a Cumulative Density Function (CDF) of the position error E_{pos}. The median error position and orientation is $0.48cm$ and 0.05° resp. and the maximum error is $0.8cm$ and 0.3° resp. Consequently, the system is accurate enough to meet the initially stated high requirements for localization systems (i.e. $1.0cm$ and 0.1° for automated driving scenarios).

B. Performance and robustness

Fig. 4 C) shows the measured timings of the marker detection algorithm ΔT_{det} and the total detection time ΔT_{total} that includes ΔT_{det} time as well as all remaining processing (e.g. loading an image from the camera, performing the homography projection, etc). In the worst case, the processing rate would be about 12Hz. Hence, real-time processing of even fast moving objects is possible.

Moreover, false positive R_{fp} and false negative rate R_{fn} of the marker detection indicate the overall robustness. Let i, j and n be the number of false, missed and total detections resp. Thus, we define $R_{fp} = \frac{i}{n}$ and $R_{fn} = \frac{j}{n}$. In our experiments, there have been incorrectly detected markers. However, the identifiers of these misdetections were not within the valid numeric range of the actual used markers and could be filtered out. Thus, both R_{fp} and R_{fn} turned out to be zero, i.e. every marker has been captured without any mismatches. Above all, illumination is a highly important factor influencing the performance of optical localization systems. We have conducted all experiments under realistic lighting conditions [3].

IV. Conclusion and Outlook

In this work, we introduced a highly accurate yet cost-effective Ground Truth system as a first building block for an automotive indoor testbed. The proposed approach relies on printable colored markers, a reference grid and customary network cameras. Furthermore, automated calibration processes significantly reduce the amount of manual effort. The proposed system is suitable for vehicles or wheeled robots, where a marker can be mounted at a fixed height. In a detailed evaluation, we determined a median error for position and orientation of $0.48cm$ and 0.05° resp. and a maximum error of $0.8cm$ and 0.3° resp. The system's detection performance proves to be highly reliable under realistic conditions.

Our long term vision is the creation of a testbed for benchmarking a vast range of localization techniques under comparable conditions. The next steps include the implementation of a standardized set of evaluation metrics reflecting different aspects of the localization performance. Moreover, it would be beneficial to equip the testbed infrastructure with additional sensors to capture environmental effects potentially influencing the localization performance. For instance, the occupancy status of all parking lots, barometric pressure and camera streams from the viewpoint of the test vehicle can be recorded. Ultimately, a replay mechanism could be implemented for testing localization algorithms with real data recorded during test runs. This would speed up development as the number of test runs can be reduced and challenging situations can be reproduced easily.

References

[1] Benjamin H Groh, Martin Friedl, Andre G Linarth, and Elli Angelopoulou. Advanced real-time indoor parking localization based on semi-static objects. In *Information Fusion (FUSION), 2014 17th International Conference on*, pages 1–7. IEEE, 2014.

[2] André Ibisch, Stefan Stumper, Harald Altinger, Marcel Neuhausen, Marc Tschentscher, Marc Schlipsing, Jan Salinen, and Alois Knoll. Towards autonomous driving in a parking garage: Vehicle localization and tracking using environment-embedded lidar sensors. In *Intelligent Vehicles Symposium (IV), 2013 IEEE*, pages 829–834. IEEE, 2013.

[3] J. Einsiedler, D. Becker, and I. Radusch. External visual positioning system for enclosed carparks. In *Positioning, Navigation and Communication (WPNC), 2014 11th Workshop on*, pages 1–6. IEEE, 2014.

[4] Jose-Luis Blanco, Francisco-Angel Moreno, and Javier Gonzalez. A collection of outdoor robotic datasets with centimeter-accuracy ground truth. *Autonomous Robots*, 27(4):327–351, 2009.

[5] Paolo Barsocchi, Stefano Chessa, Francesco Furfari, and Francesco Potorti. Evaluating ambient assisted living solutions: The localization competition. *Pervasive Computing, IEEE*, 12(4):72–79, 2013.

[6] Maarten Hooijberg. Conversions and zone systems. *Geometrical Geodesy: Using Information and Computer Technology*, pages 173–182, 2008.

[7] Gary Bradski and Adrian Kaehler. *Learning OpenCV: Computer vision with the OpenCV library*. " O'Reilly Media, Inc.", 2008.

Enabling Pedometers on Basis of Visual Feature Point Conversion

Chadly Marouane
Research & Development, VIRALITY GmbH
Rauchstraße 7
81679 Munich, Germany
Email: marouane@virality.de

Andre Ebert
Ludwig-Maximilians-Universität München
Oettingenstraße 67
80538 München, Germany
Email: andre.ebert@ifi.lmu.de

***Abstract*—Due to the rapid development of affordable, intelligent, and mobile devices, especially in the area of wearable computing (e.g., Google Glass, etc.), the implementation of applications for computational vision is more and more feasible. In this context, we propose a new concept for a pedometer, which is based on visual feature points. The introduced method is part of a visual odometry procedure, which is used for positioning on basis of optical feature points and their corresponding vectors. In order to realize the pedometer, video recordings shot from a first person perspective become analyzed. In a first step, feature points are extracted out of each of the video's frames. Subsequently, a pace movement is calculated by using the euclidian norm between equal feature points of successive frames. In the following, the concept is compared to classical pedometers, which are commonly based on an accelerometer or related inertial sensors. Besides the successful recognition of a user's paces, we take a brief look at popular techniques for feature point processing, e.g., SURF, ORB, and BRISK, regarding their suitability for visual pace detection, which is also subject of this paper. Especially their characteristics concerning robustness and computational costs for successful pace recognition are relevant in this context.**

I. Introduction

Pace recognition and its counting gained a lot of popularity during the last months. Several studies showed, that the usage of pedometers animate users to undertake more physical activities, which results in improving their health as well as the facilitation of a more healthy way of life in general [8]. Furthermore, pedometers are capable of supporting indoor positioning systems in terms of being an additional positioning sensor [6].

In order to measure the number of paces of a pedestrian, his body movements become tracked and analyzed with the help of an inertial sensor. Due to the development of today's micro controllers, it is possible to pilot inertial sensors in an electronic way. This results in them being much smaller and cheaper than their predecessors and today, it is even common that several inertial sensors are plugged into one mobile device. But despite their comprehensive distribution – due to occurring inaccuracies, inertial sensors are not suitable for all kinds of applications. Depending on the current use case, it may be reasonable to substitute them by other technologies (e.g., cameras, positioning sensors, data transmission technologies, etc.). Smartphone or body cameras are used for recording our everyday life in private as well as in work environments, e.g., the surveillance of public operations carried out by security personal. Their small and robust design enables users to record their everyday life situations from a first person perspective and in high definition quality.

After providing a brief overview across related work and technologies in Section II, we introduce a visual-based pedometer in Section III, which extracts a pedestrian's paces out of video material recorded with a body-worn action camcorder. For the pace measurement itself, a procedure based on feature point processing is used. The advantage of this method, compared to the inertial sensor-based standard procedures, is the possibility of analyzing taken video material even after its recording. Moreover, different techniques of visual feature point processing are examined concerning their suitability for pace detection. Subsequently, we present the concept's evaluation in Section IV, followed by a forecast on this matter in Section V.

II. Related Work

Classical odometry methods, based on visual analysis approaches, are enabling the estimation of a covered distance by processing video sequences. Its main area of usage is the positioning and navigation of robots or vehicles, where single cameras [12] or stereo cameras [1] as well as omni-directional cameras are used [15]. One approach for motion detection demands the cameras to be straightened into a frontal or a ground direction. Subsequently, feature points become extracted out of each frame of the taken video, in order to analyze them for match points. On basis of these feature matches, a reconstructed optical stream allows the approximation of camera motions [11]. Other approaches facilitate the calculation of changing light conditions out of the image's color and grayscale intensities instead of using feature points [5]. Originally, these methods were designed for vehicles and robots, which is why they are not suitable for the usage in combination with cameras worn by humans. Furthermore, measuring errors, evoked by different movement patterns during running or walking, do occur. While the direction of a movement can be detected in an easy way, the estimation of distances is no trivial task and leads to the need of adjusting the analysis methods for the usage with human beings. Liu et al. use approaches based on visual pedometers, similar to dead-reckoning methods for pedestrians [10]. In order to detect paces, the three movement axes are monitored by dead-reckoning to detect conspicuous accelerations [13]. In contrast, the visual pedometer counts the changes of movement directions of equal feature vectors during

a defined span of time. This increases the visual odometrie's quality of results.

III. Concept

In this section we explain our visual-based pedometer concept, which is meant to recognize and count a pedestrian's paces by analyzing video data taken with an action camcorder fastened on his body. Initially, the camera's perspective is aligned to match the user's first person view – but subsequently its installation in different positions, e.g., on the user's torso, are a matter of following examinations. The main concept of counting paces facilitates the analysis of feature points, extracted out of the recorded video material, as well as their relation to each other. DiVerdi et al. [4] and Jirawimut et al. [7] indicate, that camera movement caused by a carrier's body movement can be reconstructed by feature point extraction from successive frames and their analysis. By extending this procedure, relative movement changes of all feature points aroused by the camera's movement can be used for identifying individual pace patterns and furthermore, for recognizing the paces a user takes. Figure 1 illustrates movement changes of equal feature points in two successive frames.

Fig. 1: Vector movement of equal feature points between two successive frames.

In detail, the process is subdivided into five steps: 1) All feature points are extracted out of each frame; 2) all feature points of one frame are compared to its counterparts of the next successive frame; 3) the euclidian norm of all extracted feature points between two successive frames is calculated; 4) the euclidian norm's sign in relation of its positive or negative alterations in direction of the Y-axis is changed if necessary; 5) all values belonging to one pair of frames are summed.

Figure 2 shows the visualized course of a short sequence of a video recording taken by a pedestrian. We recorded a continuous, 10-minute-long scenario, in which one subjects walked a predefined indoor route. The video was taken with an action camcorder providing a resolution of 1920 x 1080 pixels and using the H.264 video codec. In this context, a distinct, characteristic, and reoccurring trend, which resembles the pedestrian's paces, is visible. Relying on procedures using a classical inertial sensor for modeling a pedometer [9], [10], similar jiggling patterns as well as the corresponding single paces are about to become recognized by using a feature point detection instead of an accelerometer.

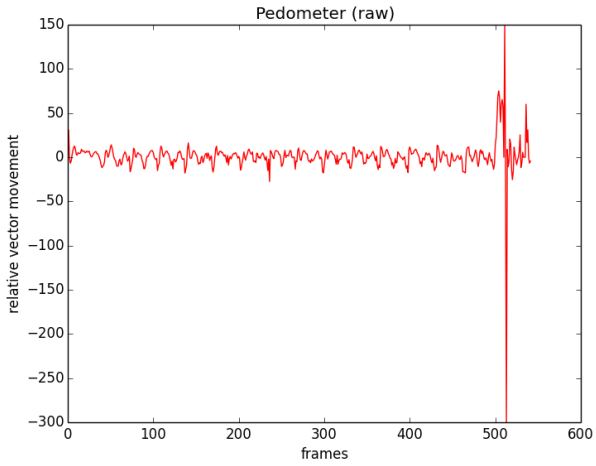

Fig. 2: Relative vector movement of the visual pedometer procedure

All in all, three different feature point procedures are utilized. Part of the examination is the question, if less robust feature point procedures are also suitable for the implementation of a pedometer. First, the popular SURF feature point procedure is used. Due to its robustness, it is one of the most well-established systems [2]. Anyways, one of its biggest disadvantages occurs during its execution. Despite several advancements and adjustments concerning the demanded resources as well as the needed execution time, its usage is computationally intensive. In contrast, at the expense of lowering the analysis' results quality, BRISK [3] and ORB [14] are faster and more resource preserving.

IV. Evaluation

For evaluation, video sequences of a walking person with an action cam on its chest, were recorded. In a first step, the challenge was to determine the number of paces taken. Figure 3 shows the results of an auto-correlated sequence, which was determined by using the visual pedometer concept. The individual paces, all in all 16 during the whole video length, are easy and clear to identify out of the given jiggling pattern. Especially the results of videos taken in the test area's straight corridors were exceptionally good.

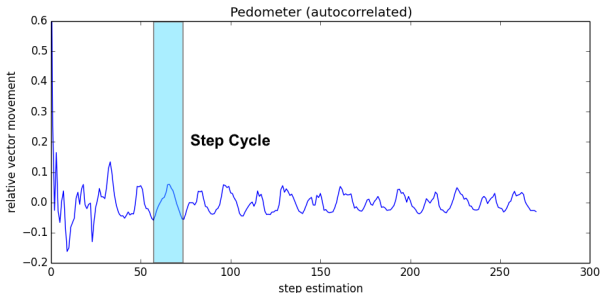

Fig. 3: Video sequence showing 16 estimated steps – auto-correlated step estimation with SURF feature detector.

In a following evaluation, we wanted to examine the performance of other feature point methods, such as ORB and BRISK, in combination with our visual pedometer concept. Because of their different needs concerning the device's resources, this matter is of particular relevance. As visualized in Figures 4a and 4b, it was not possible to reconstruct the test user's individual paces by using alternative feature point algorithms. Furthermore, even after applying an autocorrelation, a significant jiggling pattern is not detectable. A reason for that may be the lack of enough robust feature points. Moreover, because of the occurrence of to much false positive feature matches, the results are influenced negatively again. The robustness of SURF, evoked by a more strict process for matching feature points, are reasons for its successful embedding into the context of our proposed visual-based pedometer concept.

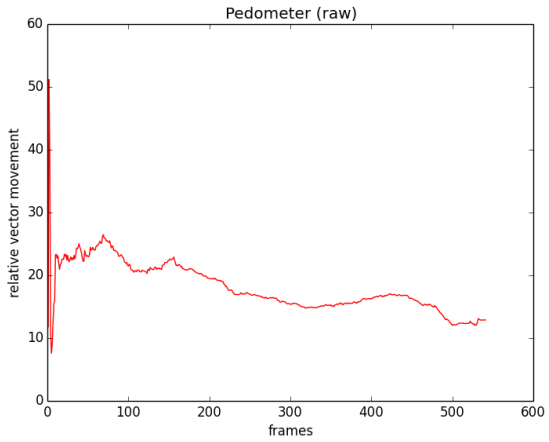

(a) BRISK

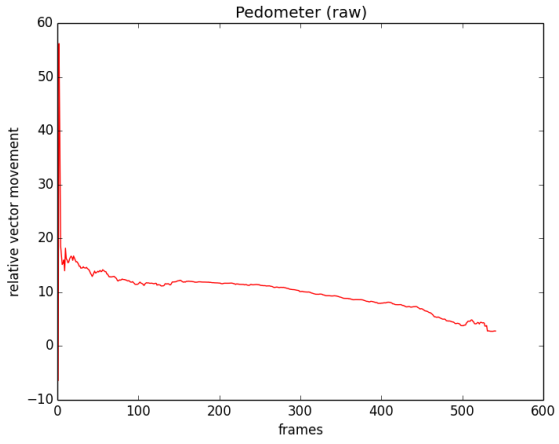

(b) ORB

Fig. 4: Relative vector movement of the visual pedometer procedure with BRISK and ORB feature detectors

V. Conclusion

Pedometers will gain a growing significance in our daily life, especially concerning the monitoring and tracking of activities as well as supporting existing indoor and outdoor positioning systems. The fundament of our proposed concept is based on the comparison of out of successive frame's extracted feature points and its visual based procedure expands the possibilities of implementing a pedometer. The video material used for the analysis is shot out of a first person perspective. Changes in movement are analyzed in respect of periodical features, which indicate single paces. Independent of the fact, that classical pedometers, which are relying on an inertial sensor, will also be indispensable in the future, our concept enables devices without an additional inertial sensor to count its user's paces by the analysis of camera data. Furthermore, existing video recordings shot from a first person perspective can be analyzed at any time without depending on the moment of their creation.

References

[1] a.I. Comport, E. Malis, and P. Rives. Real-time Quadrifocal Visual Odometry. *The International Journal of Robotics Research*, 29(2-3):245–266, 2010.

[2] H. Bay, T. Tuytelaars, and L. V. Gool. SURF : Speeded Up Robust Features.

[3] M. Calonder, V. Lepetit, C. Strecha, and P. Fua. Brief: Binary robust independent elementary features. In K. Daniilidis, P. Maragos, and N. Paragios, editors, *Computer Vision ECCV 2010*, volume 6314 of *Lecture Notes in Computer Science*, pages 778–792. Springer Berlin Heidelberg, 2010.

[4] S. DiVerdi and T. Hollerer. Heads up and camera down: A vision-based tracking modality for mobile mixed reality. *Visualization and Computer Graphics, IEEE Transactions on*, 14(3):500–512, May 2008.

[5] C. Forster, M. Pizzoli, and D. Scaramuzza. SVO : Fast Semi-Direct Monocular Visual Odometry. *IEEE International Conference on Robotics and Automation (ICRA)*, 2014.

[6] J. A. Hesch and S. I. Roumeliotis. Design and analysis of a portable indoor localization aid for the visually impaired. *Int. J. Rob. Res.*, 29(11):1400–1415, Sept. 2010.

[7] R. Jirawimut, S. Prakoonwit, F. Cecelja, and W. Balachandran. Visual odometer for pedestrian navigation. *Instrumentation and Measurement, IEEE Transactions on*, 52(4):1166–1173, Aug 2003.

[8] I. Li, A. Dey, and J. Forlizzi. Position paper on using contextual information to improve awareness of physical activity.

[9] J. Link, P. Smith, N. Viol, and K. Wehrle. Footpath: Accurate map-based indoor navigation using smartphones. In *Indoor Positioning and Indoor Navigation (IPIN), 2011 International Conference on*, pages 1–8, Sept 2011.

[10] D. Liu, Q. Shan, and D. Wu. Toward a visual pedometer. *Proceedings of the 27th Annual ACM Symposium on Applied Computing - SAC '12*, page 1025, 2012.

[11] B. D. Lucas and T. Kanade. An iterative image registration technique with an application to stereo vision. In *Proceedings of the 7th International Joint Conference on Artificial Intelligence - Volume 2*, IJCAI'81, pages 674–679, San Francisco, CA, USA, 1981. Morgan Kaufmann Publishers Inc.

[12] L. Marques. *Advances in Mobile Robotics: Proceedings of the Eleventh International Conference on Climbing and Walking Robots and the Support Technologies for Mobile Machines, Coimbra, Portugal, 8-10 September 2008*. World Scientific, 2008.

[13] Y. Murata, K. Kaji, K. Hiroi, and N. Kawaguchi. Pedestrian dead reckoning based on human activity sensing knowledge. In *Proceedings of the 2014 ACM International Joint Conference on Pervasive and Ubiquitous Computing: Adjunct Publication*, UbiComp '14 Adjunct, pages 797–806, New York, NY, USA, 2014. ACM.

[14] E. Rublee and G. Bradski. ORB : an efficient alternative to SIFT or SURF.

[15] D. Scaramuzza and R. Siegwart. Appearance-guided monocular omnidirectional visual odometry for outdoor ground vehicles. *Robotics, IEEE Transactions on*, 24(5):1015–1026, Oct 2008.

1 Detailed Program

9:00 - 9:30: Welcome and Introduction Horst Hellbrück, FH Lübeck
9:30 - 10:30: 1st. Session - Radio based Localization

- InPhase: An Indoor Localization System based on Phase Difference Measurements
  Yannic Schröder, Georg von Zengen, Stephan Rottmann, Felix Büsching, Lars Wolf
  Technische Universität Braunschweig
- Range-based Weighted-likelihood Particle Filter for RSS-based Indoor Tracking
  Zan Li, Andreea Hossmann-Picu, Torsten Braun
  University of Bern
- Towards Real-Time Network-Based Positioning in LTE
  Islam Alyafawi, Navid Nikaeiny, Torsten Braun
  Universität Bern

10:30 - 11:00: Coffee break
11:00 - 12:00: 2nd. Session - Localization using Topology

- Adhoc Topology retrival using USRP
  Chuong Thach Nguyen, Stephan Sigg, Xiaoming Fu
  University of Goettingen
- Topological Localization with Bluetooth Low Energy in Office Buildings
  Julian Lategahn, Thomas Ax, Marcel Müller, Christof Röhrig
  University of Applied Sciences and Arts in Dortmund
- Clustering of Inertial Indoor Positioning Data
  Lorenz Schauer, Martin Werner
  Ludwig-Maximilians Universität

12:00 - 13:00: Lunch break
13:00 - 14:00: 3rd. Session - Visual Localization

- Lane-Level Localization on Lanelet Maps Using Production Vehicle Sensors
  Johannes Rabe, Sascha Quell, Marc Necker, Christoph Stiller
  Daimler AG, Karlsruhe Institute of Technology
- Testbed for automotive indoor localization
  Daniel Becker, Fabian Thiele, Oliver Sawade, Ilja Radusch
  Daimler Center for Automotive Information Technology
- Enabling Pedometers on Basis of Visual Feature Point Conversion
  Chadly Marouane, Andre Ebert
  Research & Development VIRALITY GmbH, Ludwig-Maximilians-Universität München

14:00 - 14:30: Coffee break
14:30 - 14:50: Closing, Wrap-up and open discussion

2 Aachener Informatik-Berichte

This list contains all technical reports published during the past three years. A complete list of reports dating back to 1987 is available from:

`http://aib.informatik.rwth-aachen.de/`

To obtain copies please consult the above URL or send your request to:

Informatik-Bibliothek, RWTH Aachen, Ahornstr. 55, 52056 Aachen,
Email: `biblio@informatik.rwth-aachen.de`

2012-01 Fachgruppe Informatik: Annual Report 2012

2012-02 Thomas Heer: Controlling Development Processes

2012-03 Arne Haber, Jan Oliver Ringert, Bernhard Rumpe: MontiArc - Architectural Modeling of Interactive Distributed and Cyber-Physical Systems

2012-04 Marcus Gelderie: Strategy Machines and their Complexity

2012-05 Thomas Ströder, Fabian Emmes, Jürgen Giesl, Peter Schneider-Kamp, and Carsten Fuhs: Automated Complexity Analysis for Prolog by Term Rewriting

2012-06 Marc Brockschmidt, Richard Musiol, Carsten Otto, Jürgen Giesl: Automated Termination Proofs for Java Programs with Cyclic Data

2012-07 André Egners, Björn Marschollek, and Ulrike Meyer: Hackers in Your Pocket: A Survey of Smartphone Security Across Platforms

2012-08 Hongfei Fu: Computing Game Metrics on Markov Decision Processes

2012-09 Dennis Guck, Tingting Han, Joost-Pieter Katoen, and Martin R. Neuhäußer: Quantitative Timed Analysis of Interactive Markov Chains

2012-10 Uwe Naumann and Johannes Lotz: Algorithmic Differentiation of Numerical Methods: Tangent-Linear and Adjoint Direct Solvers for Systems of Linear Equations

2012-12 Jürgen Giesl, Thomas Ströder, Peter Schneider-Kamp, Fabian Emmes, and Carsten Fuhs: Symbolic Evaluation Graphs and Term Rewriting — A General Methodology for Analyzing Logic Programs

2012-15 Uwe Naumann, Johannes Lotz, Klaus Leppkes, and Markus Towara: Algorithmic Differentiation of Numerical Methods: Tangent-Linear and Adjoint Solvers for Systems of Nonlinear Equations

2012-16 Georg Neugebauer and Ulrike Meyer: SMC-MuSe: A Framework for Secure Multi-Party Computation on MultiSets

2012-17 Viet Yen Nguyen: Trustworthy Spacecraft Design Using Formal Methods

2013-01 * Fachgruppe Informatik: Annual Report 2013

2013-02 Michael Reke: Modellbasierte Entwicklung automobiler Steuerungssysteme in Klein- und mittelständischen Unternehmen

2013-03 Markus Towara and Uwe Naumann: A Discrete Adjoint Model for OpenFOAM

2013-04 Max Sagebaum, Nicolas R. Gauger, Uwe Naumann, Johannes Lotz, and Klaus Leppkes: Algorithmic Differentiation of a Complex C++ Code with Underlying Libraries

2013-05 Andreas Rausch and Marc Sihling: Software & Systems Engineering Essentials 2013

2013-06 Marc Brockschmidt, Byron Cook, and Carsten Fuhs: Better termination proving through cooperation

2013-07 André Stollenwerk: Ein modellbasiertes Sicherheitskonzept für die extrakorporale Lungenunterstützung

2013-08 Sebastian Junges, Ulrich Loup, Florian Corzilius and Erika Ábrahám: On Gröbner Bases in the Context of Satisfiability-Modulo-Theories Solving over the Real Numbers

2013-10 Joost-Pieter Katoen, Thomas Noll, Thomas Santen, Dirk Seifert, and Hao Wu: Performance Analysis of Computing Servers using Stochastic Petri Nets and Markov Automata

2013-12 Marc Brockschmidt, Fabian Emmes, Stephan Falke, Carsten Fuhs, and Jürgen Giesl: Alternating Runtime and Size Complexity Analysis of Integer Programs

2013-13 Michael Eggert, Roger Häußling, Martin Henze, Lars Hermerschmidt, René Hummen, Daniel Kerpen, Antonio Navarro Pérez, Bernhard Rumpe, Dirk Thißen, and Klaus Wehrle: SensorCloud: Towards the Interdisciplinary Development of a Trustworthy Platform for Globally Interconnected Sensors and Actuators

2013-14 Jörg Brauer: Automatic Abstraction for Bit-Vectors using Decision Procedures

2013-16 Carsten Otto: Java Program Analysis by Symbolic Execution

2013-19 Florian Schmidt, David Orlea, and Klaus Wehrle: Support for error tolerance in the Real-Time Transport Protocol

2013-20 Jacob Palczynski: Time-Continuous Behaviour Comparison Based on Abstract Models

2014-01 * Fachgruppe Informatik: Annual Report 2014

2014-02 Daniel Merschen: Integration und Analyse von Artefakten in der modellbasierten Entwicklung eingebetteter Software

2014-03 Uwe Naumann, Klaus Leppkes, and Johannes Lotz: dco/c++ User Guide

2014-04 Namit Chaturvedi: Languages of Infinite Traces and Deterministic Asynchronous Automata

2014-05 Thomas Ströder, Jürgen Giesl, Marc Brockschmidt, Florian Frohn, Carsten Fuhs, Jera Hensel, and Peter Schneider-Kamp: Automated Termination Analysis for Programs with Pointer Arithmetic

2014-06 Esther Horbert, Germán Martín García, Simone Frintrop, and Bastian Leibe: Sequence Level Salient Object Proposals for Generic Object Detection in Video

2014-07 Niloofar Safiran, Johannes Lotz, and Uwe Naumann: Algorithmic Differentiation of Numerical Methods: Second-Order Tangent and Adjoint Solvers for Systems of Parametrized Nonlinear Equations

2014-08 Christina Jansen, Florian Göbe, and Thomas Noll: Generating Inductive Predicates for Symbolic Execution of Pointer-Manipulating Programs

2014-09 Thomas Ströder and Terrance Swift (Editors): Proceedings of the International Joint Workshop on Implementation of Constraint and Logic Programming Systems and Logic-based Methods in Programming Environments 2014

2014-14 Florian Schmidt, Matteo Ceriotti, Niklas Hauser, and Klaus Wehrle: HotBox: Testing Temperature Effects in Sensor Networks

2014-15 Dominique Gückel: Synthesis of State Space Generators for Model Checking Microcontroller Code

2014-16 Hongfei Fu: Verifying Probabilistic Systems: New Algorithms and Complexity Results

2015-01 * Fachgruppe Informatik: Annual Report 2015

2015-05 Florian Frohn, Jürgen Giesl, Jera Hensel, Cornelius Aschermann, and Thomas Ströder: Inferring Lower Bounds for Runtime Complexity

2015-06 Thomas Ströder and Wolfgang Thomas (Editors): Proceedings of the Young Researchers' Conference "Frontiers of Formal Methods"

2015-07 Hilal Diab: Experimental Validation and Mathematical Analysis of Cooperative Vehicles in a Platoon

2015-09 Xin Chen: Reachability Analysis of Non-Linear Hybrid Systems Using Taylor Models

* These reports are only available as a printed version.

Please contact `biblio@informatik.rwth-aachen.de` to obtain copies.